HHS Public Access

Author manuscript

Neuron. Author manuscript; available in PMC 2023 August 03.

Published in final edited form as:

Neuron. 2022 August 03; 110(15): 2422–2437.e9. doi:10.1016/j.neuron.2022.05.009.

Neuronal NLRP3 is a parkin substrate that drives neurodegeneration in Parkinson's Disease

Nikhil Panicker[1,2], **Tae-In Kam**[1,2,7], **Hu Wang**[1,2,8], **Stewart Neifert**[1,2,7,8], **Shih-Ching Chou**[1,3], **Manoj Kumar**[1,2], **Saurav Brahmachari**[1,2], **Aanishaa Jhaldiyal**[1,4], **Jared T. Hinkle**[1,5], **Fatih Akkentli**[1,2,7,8], **Xiaobo Mao**[1,2], **Enquan Xu**[1,2], **Senthilkumar S. Karuppagounder**[1,2], **Eric T. Hsu**[5], **Sung Ung Kang**[1,2], **Olga Pletnikova**[6], **Juan Troncoso**[2,6], **Valina L. Dawson**[1,2,4,5,7,8,*,#], **Ted M. Dawson**[1,2,3,5,7,8,9,*,#]

[1]Neuroregeneration and Stem Cell Programs, Institute for Cell Engineering, Johns Hopkins University School of Medicine, Baltimore, MD 21205, USA

[2]Department of Neurology, Johns Hopkins University School of Medicine, Baltimore, MD 21205, USA

[3]Department of Pharmacology and Molecular Sciences, Johns Hopkins University School of Medicine, Baltimore, MD 21205, USA

[4]Department of Physiology, Johns Hopkins University School of Medicine, Baltimore, MD 21205, USA

[5]Solomon H. Snyder Department of Neuroscience, Johns Hopkins University School of Medicine, Baltimore, MD 21205, USA

[6]Department of Pathology, Johns Hopkins University School of Medicine, Baltimore, MD 21205, USA

[7]Diana Helis Henry Medical Research Foundation, New Orleans, LA 70130, USA

[8]Adrienne Helis Malvin Medical Research Foundation, New Orleans, LA 70130, USA

[9]Lead Contact

Summary

[*]Correspondence to: Valina L. Dawson, Ph.D. (vdawson@jhmi.edu) or Ted M. Dawson, M.D., Ph.D. (tdawson@jhmi.edu).
[#]These authors contributed equally.

Author contributions

Conceptualization: N.P, V.L.D & T.M.D, Methodology: N.P, T-I.K V.L.D & T.M.D, Formal Analysis: N.P, Investigation: N.P, T-I.K, H.W, S.N, M.K, S.B, A.J, J.T.H, F.A, X.M, E.X, S.S.K, E.T.H, S-U.K, O.P, J.T., Writing-Review & Editing: N.P, V.L.D & T.M.D, Funding Acquisition: N.P, V.L.D & T.M.D, Supervision, V.L.D. and T.M.D. All authors have read and approved the final manuscript.

Declaration of Interests

The value of patents owned by Valted, LLC could be affected by the study described in this article. Dr. T. and V. Dawson are founders of Valted, LLC and hold an ownership equity interest in the company. This arrangement has been reviewed and approved by the Johns Hopkins University in accordance with its conflict-of-interest policies.

INCLUSION AND DIVERSITY

For studies involving non-human subjects or material, we worked to ensure sex balance in the selection of non-human subjects.

Parkinson's disease (PD) is mediated, in part, by intraneuronal accumulation of α-synuclein aggregates and subsequent death of dopamine (DA) neurons in the substantia nigra *pars compacta* (SNpc). Microglial hyperactivation of the Nod-Like Receptor Protein-3 (NLRP3) inflammasome has been well-documented in various neurodegenerative diseases, including PD. We show here that loss of parkin activity in mouse and human DA neurons results in spontaneous neuronal NLRP3 inflammasome assembly, leading to DA neuron death. Parkin normally inhibits inflammasome priming by ubiquitinating and targeting NLRP3 for proteasomal degradation. Loss of parkin activity also contributes to assembly of active NLRP3 inflammasome complex via mitochondrial-derived reactive oxygen species (mitoROS) generation through the accumulation of another parkin ubiquitination substrate, ZNF746/PARIS. Inhibition of neuronal NLRP3 inflammasome assembly prevents degeneration of DA neurons in familial and sporadic PD models. Strategies aimed at limiting neuronal NLRP3 inflammasome activation hold promise as a disease modifying therapy for PD.

eTOC blurb

Inflammasomes are multimeric signaling platforms traditionally shown to be assembled in immune cells. Here, Panicker et al., shows inactivation of the E3 ligase parkin from dopamine neurons results in spontaneous activation of the neuronal NLRP3 inflammasome, contributing to dopamine neuron death and neurodegeneration in Parkinson's disease.

Graphical Abstract

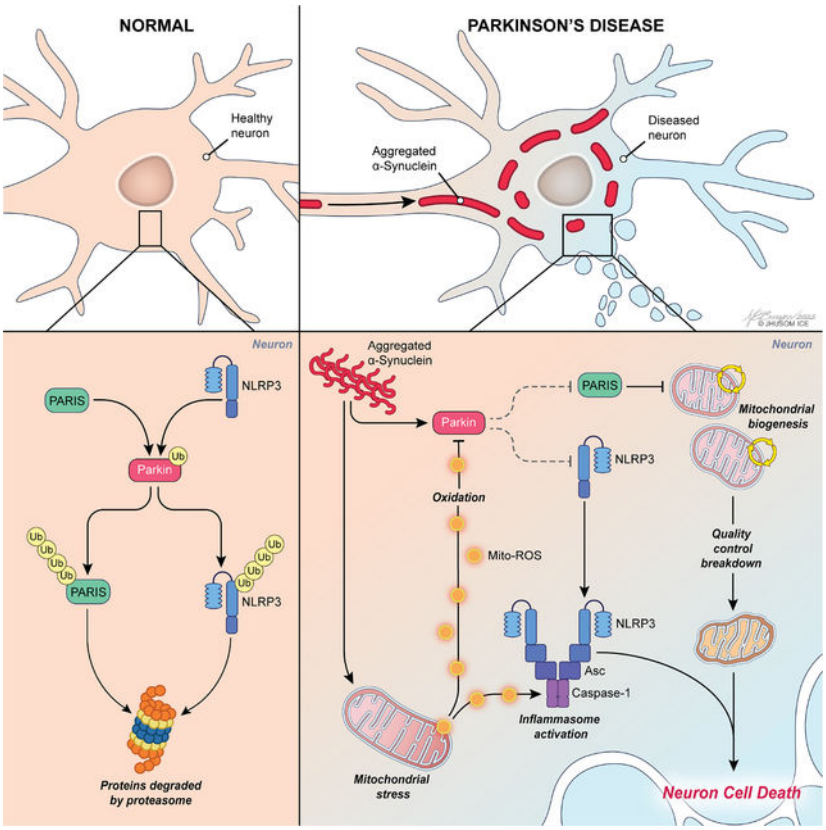

Keywords

Parkinson's disease; NLRP3; Caspase-1; parkin; Inflammasome; ubiquitination; neurodegeneration

Introduction

The preferential death of dopamine (DA) neurons in the substantia nigra *pars compacta* (SNpc) is a hallmark of Parkinson's Disease (PD). Depletion of DA in the striatum (the region of the brain to which the SNpc DA neurons project) is accompanied by motor deficits, including bradykinesia and resting tremors (Dauer and Przedborski, 2003; Pirooznia et al., 2021; Savitt et al., 2006). There are currently no disease-modifying therapies that slow PD progression. Intraneuronal accumulation of pathologic α-Synuclein (α-Syn) and mitochondrial dysfunction are among the known contributors to PD pathology (Di Maio et al., 2016; Exner et al., 2012; Moon and Paek, 2015; Scarffe et al., 2014).

Several genes whose mutations cause monogenic PD encode proteins that play crucial roles in mitochondrial quality control (Ge et al., 2020). These include *PRKN*, which codes for the E-3 ubiquitin ligase parkin (Kitada et al., 1998). Damaged mitochondria release reactive oxygen species (mitoROS) as a result of electron transport chain dysfunction (Turrens, 2003). The NLRP3 inflammasome, a major component of the innate-immune system, is a three-protein complex comprised of the cytosolic pattern-recognition receptor NLRP3, the adaptor-protein ASC, and Caspase-1 (Casp1). The assembly of this complex is triggered by pathogenic infection as well as sterile inflammogens (Swanson et al., 2019). We and others have demonstrated that microglial NLRP3 inflammasome hyperactivation results in a sterile inflammatory response that contributes to PD pathology (Gordon et al., 2018; Panicker et al., 2019). The pathologic role for neuronal inflammasome activation in the context of neurodegenerative disease is yet to be elucidated, though neuronal assembly of the AIM2 inflammasome was recently implicated in synapse elimination during neurodevelopment (Lammert et al., 2020).

The NLRP3 inflammasome requires two signals -priming and activation - for complete assembly. Priming (signal-1) entails the induction of the NLRP3 protein. Activation (signal-2) is initiated by the production of mitoROS and culminates in the oligomerization of the inflammasome adaptor protein ASC, formation of ASC specks, and autoproteolytic activation of the effector inflammasome protease Casp1. Since mitochondrial dysfunction is prominent in DA neurons degenerating in PD (Exner *et al.*, 2012), we hypothesized that the NLRP3 inflammasome could become activated in DA neurons, driving their loss in a cell autonomous manner.

We show here that loss of parkin activity in DA neurons results in spontaneous NLRP3 inflammasome priming and assembly, leading to degeneration of DA neurons in adult conditional parkin knockouts and α-Syn pre-formed fibril (PFF) mouse models of PD. Moreover, we show that NLRP3 is a parkin substrate and that parkin normally inhibits inflammasome priming (signal-1) by ubiquitinating NLRP3, designating it for proteasomal degradation. Loss of parkin function also contributes to activation of the NLRP3 complex

(signal-2) by via the accumulation of the parkin-interacting substrate (PARIS), ZNF746, which contributes to mitoROS generation. Furthermore, inhibition of NLRP3 inflammasome function prevents degeneration of DA neurons. Strategies aimed at inhibiting NLRP3 inflammasome activation through maintaining parkin activity therefore hold promise as disease modifying therapies to treat PD.

Results

NLRP3 inflammasome is activated within DA neurons following parkin depletion

Stereotaxic injection of AAV GFP-Cre constructs into the SNpc of parkin$^{flx/flx}$ mice results in adult-onset, SNpc DA-neuron specific parkin depletion. This triggers a decline in mitochondrial function and mass that results in DA neuron death (Shin et al., 2011; Stevens et al., 2015). Inflammasome priming and activation under these conditions were assessed by immunoblot analysis of ventral midbrain lysates of AAV GFP- or AAV GFP-Cre-injected parkin$^{flx/flx}$ mice (scheme provided in Fig. 1A). We observed depletion of parkin in AAV GFP-Cre injected samples, and a simultaneous increase in levels of both NLRP3 and cleaved Casp1, suggesting that the NLRP3 inflammasome was primed and activated in the absence of parkin (Fig. 1B). We confirmed inflammasome activation was not a result of microglial or monocytic cells by using immunohistochemistry (IHC). Stereotaxic injection of AAVs into the SNpc resulted in ~80% targeting of SNpc DA neurons (assessed *via* co-localization of the GFP signal with tyrosine hydroxylase/TH, a DA neuron marker). Very few (~ 5%) microglia in the region were transduced, as assessed by Iba-1 /GFP colocalization (Fig. S1A). To validate that DA-neuron parkin deletion was eliciting cell-autonomous inflammasome activation, a FLuorochrome Inhibitor of CAspases (FLICA) assay was performed to assess Casp1 activity in ventral midbrain sections of AAV GFP- or AAV GFP-Cre-injected parkin$^{flx/flx}$ mice, coupled with immunostaining sections for TH and Iba-1. These experiments revealed that parkin depletion results in a significant upregulation of Casp1 activity in SNpc DA neurons, but not in microglia (Fig. 1C), indicating that neuronal depletion of parkin leads to cell-autonomous activation of the NLRP3 inflammasome. IHC analysis also revealed upregulation of NLRP3 (Fig S1B) and formation of ASC-specks (Fig. 1D), which are markers of inflammasome assembly in parkin depleted DA neurons, but not in microglia. q-RT PCR revealed no change in NLRP3 and Casp1 mRNA levels in AAV GFP- and AAV GFP-Cre-injected parkin$^{flx/flx}$ mice, suggesting that parkin was modulating NLRP3 at the protein level (Fig 1E). Next, we depleted microglia in parkin$^{flx/flx}$ mice by administering the orally active, brain penetrant CSF1R inhibitor PLX5622 incorporated into the feed. Control feed was administered to littermate parkin$^{flx/flx}$ mice. These mice were then subjected to adult-onset DA neuron parkin depletion, which led to statistically similar NLRP3 and cleaved Casp1 induction (Fig. 1F), as well as unchanged DA neuron FLICA levels (Fig. 1G) in both treatment groups.

In PARKIN deficient human DA (hDA) neurons (Kumar et al., 2020) immunoblot analysis showed increased NLRP3 and cleaved Casp1 levels compared to isogenic control (iCont) hDA neurons (Fig. 1H). A Disuccinimidyl Suberate (DSS)-crosslinking assay revealed ASC oligomerization in PARKIN-deficient hDA neurons versus iCont hDA neurons, indicating assembly of the NLRP3 complex (Fig. 1I). These results were supported by

increased FLICA signal/ Casp1 activity (Fig. 1J) and staining for NLRP3 (Fig. S1C) in the PARKIN-deficient hDA neurons versus iCont hDA neurons. PARKIN-deficient hDA neurons displayed elevated mitoROS levels compared to iCont hDA neurons (Fig. S1D). NLRP3 inflammasome activation in PARKIN-deficient hDA neurons did not result in a detectable IL-1β or IL-18 response in the supernatant (Fig. S1E). Lipopolysaccharide (LPS) is known to elicit NLRP3 induction in myeloid cells but was unable to do so in either iCont or PARKIN-deficient hDA neurons (treated with 1 μg/mL LPS for 24 h) (Fig. S1F), suggesting that the cellular mechanisms leading to NLRP3 inflammasome priming in DA neurons may differ from canonical NLRP3 inflammasome priming pathways explored in myeloid cells. Next, we observed significant induction of Gasdermin-D cleavage in both adult-onset DA neuron-specific parkin depleted mice, as well as in PARKIN-deficient hDA neurons (Fig. S1G, H). The levels of the parkin/PINK1 associated protein Htra2 did not show any changes under these conditions (Fig. S1G, H).

Adult-onset NLRP3 inflammasome activation within DA neurons is sufficient to drive DA neuron loss

We used the Nlrp3^{A350VneoR} mouse line that expresses the Muckle-Wells associated A350V mutant NLRP3 gene (resulting in constitutively active NLRP3) in Cre-recombinase expressing cells to assess the effect of SNpc DA neuron NLRP3 inflammasome activation (Brydges et al., 2009). AAV GFP or AAV GFP-Cre was stereotaxically injected into the SNpc of 8–10-week-old Nlrp3^{A350VneoR} mice for 3 months, as indicated in the scheme in Fig. 2A. Triple-staining IHC verified successful transduction of TH-expressing dopaminergic SNpc neurons as ~ 80 % of TH neurons were positive for GFP, while there was minimal overlap of the GFP signal in Iba-1 positive microglia (Fig. 2B, C). Adult-onset, SNpc DA-neuron specific activation of the NLRP3 complex resulted in a robust inflammasome response as revealed by immunoblot analysis of Casp1 cleavage (Fig. 2D) and increased FLICA activity within TH-positive DA neurons but not Iba1-positive microglia (Fig. S2A), culminating in DA neuron loss, as assessed by stereologic counting of TH- and Nissl-positive neurons when compared to the AAV GFP-injected side (Fig. 2E, F). DA neuron death was accompanied by onset of motor deficits, verified by amphetamine-induced rotation testing (Fig. S2B, Video S1). These results suggest that cell autonomous NLRP3 inflammasome activation is sufficient to drive DA neuron death.

Parkin polyubiquitinates neuronal NLRP3, targeting it for proteasomal clearance

It is hypothesized that the NLRP3 inflammasome evolved a two-step activation mechanism to prevent its unintended assembly (Lamkanfi and Dixit, 2014). Canonical inflammasome priming, entails the induction of the cytosolic receptor NLRP3. After observing increased NLRP3 protein but not mRNA in parkin deficient conditions, we sought to assess whether parkin and NLRP3 proteins might interact. We found that myc-tagged parkin and FLAG-tagged NLRP3 co-immunoprecipitated in SH-SY5Y cells (Fig. S3A). GST pulldown assays verified that GST-tagged parkin could pull down recombinant NLRP3 protein, showing that the proteins could directly interact (Fig. 3A). Parkin co-immunoprecipitated with NLRP3 in ventral midbrain lysates of WT, but not parkin$^{-/-}$ or NLRP3$^{-/-}$ mice (Fig. 3B). We used truncated NLRP3 and parkin constructs to map out the interaction of these proteins. Domain structures of the full-length and truncated FLAG-NLRP3 constructs are shown in

Fig. S3B. FLAG-tagged NBD and LRR domains of NLRP3, but not the FLAG-PYD domain could pull down myc-parkin (Fig. S3C). Myc-parkin could only pull down the FLAG-NBD domain of NLRP3 (Fig. S3C). Domain structures of the myc-parkin constructs are shown in Fig. S3D. The myc-tagged RING2 and IBR-RING2 domains of parkin could pull down FLAG-tagged NLRP3 equivalent to WT parkin (Fig. S3E). Reciprocally, FLAG-tagged NLRP3 could co-immunoprecipitate myc-tagged RING2 and DUBL-parkin (Fig. S3E).

FLAG-tagged NLRP3 could be ubiquitinated by myc-tagged parkin in SH-SY5Y cells, as indicated by a smear of HA signal for HA-Ubiquitin (Fig. 3C). The FLAG signal also displayed a smearing pattern, providing further evidence of parkin-mediated NLRP3 polyubiquitination (Fig. 3C). Constructs encoding familial C431S parkin, which lacks E-3 ligase activity, or a mutant HA where all the lysine residues have been mutated to arginine residues that cannot incorporate into polyubiquitin chains, prevented parkin-mediated NLRP3 ubiquitination (Fig. 3C). An in-cell ubiquitination assay was used to show that parkin could ubiquitinate the NBD domain of NLRP3, but not other NLRP3 domains (Fig. S3F). HA and FLAG signals were visualized in different channels using fluorescent western blots. A polyubiquitinated smearing pattern was observed with both full-length FLAG-NLRP3 and NBD-FLAG-NLRP3 (Fig. S3F).

In vitro ubiquitination assays were set up to demonstrate recombinant parkin-mediated NLRP3 ubiquitination. Parkin maintains an autoinhibited conformation, requiring PINK1 kinase activity to attain functionality (Kane et al., 2014; Wauer and Komander, 2013). Human PINK1 displays low kinase activity. Tribolium castaneum (Tc) PINK1 on the other hand has substantial kinase activity which can be utilized in *in vitro* kinase assays (Woodroof et al., 2011). TcPINK1 activated WT parkin, which ubiquitinates recombinant NLRP3 protein. Parkin auto-ubiquitination as well as NLRP3 ubiquitination were abolished with inactive TcPINK1 or mutant C431S parkin (Fig. 3D). Since parkin ubiquitinates itself, we assessed parkin/NLRP3 ubiquitination in the presence and absence of TcPINK1 and NLRP3 (Fig. S3G). Detection of NLRP3 ubiquitination only occurs in the presence of both TcPINK1 and NLRP3, while auto-ubiquitination of parkin is detected in either setting (Fig. S3G). We utilized the Tandem Ubiquitin Binding Entities (TUBE) assay (Seo et al., 2021) to provide evidence that DA neuron NLRP3 is a parkin polyubiquitination substrate. TUBE pulldown resulted in an NLRP3 signal in iCont, but not in PARKIN-deficient hDA neurons, and in AAV-GFP-injected, but not AAV-GFP-Cre injected parkin$^{flx/flx}$ ventral midbrain lysates (Fig. 3E, F). To show that the parkin-mediated polyubiquitination led to its clearance, we utilized Cycloheximide (CHX) chase assays. The half-life of FLAG-NLRP3 was significantly decreased in SH-SY5Y cells co-transfected with FLAG-NLRP3 and myc-tagged WT parkin, while myc-C431S parkin overexpression increased FLAG-NLRP3 half-life (Fig. 3G). We performed CHX chase assays in iCont and in PARKIN-deficient hDA neurons, which showed that NLRP3 half-life was substantially higher in the absence of PARKIN (Fig. 3H). WT-parkin mediated FLAG-NLRP3 clearance could be reversed following pre-treatment with the proteasome inhibitor MG-132 (Fig. S3H), suggesting that parkin mediates the clearance of NLRP3 via the proteasome. Taken together these results indicate that DA neuronal parkin ubiquitinates NLRP3 within the NBD domain, targeting it for proteasomal degradation.

Accumulation of the Parkin-Interacting Substrate ZNF746 (PARIS) facilitates NLRP3 inflammasome assembly *via* mitoROS production

Previous studies have demonstrated that PARIS-mediated inhibition of mitochondrial biogenesis leads to many of the mitochondrial deficits that occur under parkin deficiency (Jo et al., 2021; Kumar *et al.*, 2020; Pirooznia et al., 2022; Pirooznia et al., 2020; Shin *et al.*, 2011; Stevens *et al.*, 2015). Since mitochondrial dysfunction-mediated mitoROS production is necessary and sufficient for NLRP3 inflammasome activation (Zhou et al., 2011), we assessed the role of PARIS in DA neuron inflammasome activation. We introduced AAV shRNA-PARIS (or AAV con-shRNA) along with AAV GFP-Cre into parkin$^{flx/flx}$ mice to prevent PARIS induction following parkin deletion (Fig. 4A). The FLICA assay, followed by staining for TH and Iba-1 demonstrated a marked reduction of DA neuron Casp1 activity in mice that were co-injected with the AAV GFP-Cre and AAV shRNA-PARIS constructs (Fig. 4B). The FLICA Casp1 activity assay was corroborated by immunoblot data, which showed a significant decline in cleaved Casp1 as well as cleaved Gasdermin-D levels in ventral midbrain lysates of parkin$^{flx/flx}$ mice that were co-injected with the AAV GFP-Cre and AAV shRNA-PARIS constructs when compared to parkin$^{flx/flx}$ mice injected with AAV GFP-Cre + AAV con-shRNA (Fig. 4C). Immunoblot analysis also confirmed the KO of parkin following the AAV GFP-Cre injection and the knockdown of PARIS following the AAV shRNA-PARIS (Fig. 4C). The induction of NLRP3 was not significantly altered between these two groups, suggesting that DA neuron inflammasome priming and activation are independent processes (Fig. 4C). Consistent with prior observations, preventing PARIS accumulation also protected mice from DA neuron degeneration as determined by stereological counting for TH-positive DA neurons and Nissl positive neurons in the SNpc (Fig. S4B, C). To assess NLRP3 inflammasome priming and activation under PARIS knockdown conditions in hDA neurons, we employed the DSS-crosslinking assay and immunoblotting and found a marked attenuation of ASC oligomerization as well as Casp1 and Gasdermin-D cleavage in the PARKIN-deficient hDA neurons lines where PARIS was also knocked down (Fig. 4D). PARIS knockdown did not affect NLRP3 induction in PARKIN-deficient hDA neurons. MitoSOX Red staining was coupled with TH immunocytochemistry (ICC) to validate that PARIS knockdown abrogated PARKIN-deficiency induced increase in mitoROS accumulation (Fig. S4A). FLICA staining, coupled with ICC for TH, verified that reducing PARIS levels prevented Casp1 activation in parkin-deficient hDA lines (Fig. 4E). These results indicate that PARIS is required for step-2 of the NLRP3 inflammasome activation pathway in DA neurons in the setting of knockout of parkin.

Preventing inflammasome activation protects loss of parkin-associated neurodegeneration

We sought to identify NLRP3 as the major inflammasome sensor that drives DA neuron Casp1 activation under parkin deficiency. We introduced AAV NLRP3-shRNA (or non-targeting AAV control shRNA) along with AAV GFP-Cre into parkin$^{flx/flx}$ mice to prevent NLRP3 induction following parkin deletion. The *in vivo* knockdown of NLRP3 completely abrogated Casp1 activation, assessed *via* immunoblot analysis of ventral midbrain lysates (Fig. 5A) and FLICA staining coupled with TH IHC (Fig. S5A, C). We utilized immunoblots and IHC to confirm NLRP3 knockdown in DA neurons but not in microglia (Fig. 5A, S5B, C). Reducing DA neuron NLRP3 prevented adult-onset

parkin deletion mediated DA neuron loss, as assessed *via* TH/Nissl staining and stereology analysis (Fig. 5B, C). Knockout of PARKIN in hDA neurons leads to a reduction in TH expression and death of these neurons as determined by propidium iodide (PI) staining consistent with our previous studies (Kumar *et al.*, 2020). We utilized these assays to demonstrate that NLRP3 inflammasome-specific inhibitor compound MCC-950 could prevent neuron death and restore TH expression in PARKIN-deficient hDA neurons (Fig. S5 D–G). Inflammasome activation culminates in the autoproteolytic activation of Casp1, the effector protease of the inflammasome complex (Lamkanfi and Dixit, 2014). Inhibiting Casp1 constrains inflammasome function. We bred parkin$^{flx/flx}$ mice with Casp1$^{-/-}$ mice to obtain parkin$^{flx/flx}$/ Casp1$^{-/-}$ and littermate control parkin$^{flx/flx}$/ Casp1$^{+/+}$ mice. Immunoblot analysis of ventral midbrain lysates from these mice confirmed adult-onset parkin depletion as well as Casp1 knockout in the double transgenic mice (Fig. S6A). These mice were subjected to adult-onset DA neuron parkin depletion with stereotaxic AAV GFP or AAV GFP-Cre SNpc injection. Three months post injection, stereological counting of TH/Nissl-stained brain sections. AAV GFP-Cre-injected parkin$^{flx/flx}$/ Casp1$^{-/-}$ mice showed significant neuroprotection and preservation of TH positive DA neurons compared to their littermate counterparts (Fig. 5D and 5E). The FLICA assay confirmed complete loss of Casp1 activity in the ventral midbrain sections of AAV GFP- and AAV GFP-Cre-injected parkin$^{flx/flx}$/ Casp1$^{-/-}$ mice (Fig. S6B). It should be noted that a few non-TH positive cells in the SNpc of AAV GFP-Cre-injected parkin$^{flx/flx}$/ Casp1$^{+/+}$ mice were also FLICA positive (marked with yellow arrows), although these could also be dead or dying DA neurons that have lost TH expression (Fig. S6B). Lentiviral CRISPR/Cas9 mediated gene editing was employed to downregulate Casp1 expression in iCont and PARKIN deficient hDA neurons. Two CRISPR constructs were designed to target the 5' UTR and Exon-2 of Casp1. Screening in SH-SY5Y cells indicated that the Exon-2 construct was more effective in abolishing Casp1 expression (Fig. S6C). The Exon-2 Casp1 construct mediated a dose-dependent reduction in Casp1 levels in iCont as well as in the two PARKIN deficient hDA neuron cell lines as assessed by immunoblotting for Casp1 (Fig. S6D). NLRP3 levels were unaffected by the Casp1 constructs (Fig. S6D). Knockdown of Casp1 prevented the reduction of TH expression as well as cell death in PARKIN-deficient hDA neurons (Fig. 5F–I).

Loss of parkin activity licenses DA neuron NLRP3 inflammasome activation in the α-Syn PFF model

The majority of PD cases are sporadic in nature, occurring in individuals without family history of the disease. Self-templated spread of α-Syn pathology between neuroanatomically connected brain regions is emerging as an important underlying pathogenic mechanism in sporadic PD (Henderson et al., 2019). This prionic spread of pathologic α-Syn is modeled through the injection of α-Syn PFFs into the mouse striatum (Luk et al., 2012). Parkin is inactivated following α-Syn PFF injection, which leads to an accumulation of parkin substrates and mitochondrial deficits (Brahmachari et al., 2019). We confirmed that an intrastriatal injection of α-Syn PFFs leads to reduction in parkin activity in the ventral midbrain as assessed by parkin autoubiquitination (Fig. 6A). The detection of serine 129-phosphorylated α-Syn (pS129-α-Syn, a marker of pathologic α-Syn) by immunoblot analysis in the ventral midbrain is consistent with the templating and propagation of

α-Syn (Fig. 6B). Accompanying the reduction in parkin activity is NLRP3 priming, and activation as demonstrated by a significant upregulation of NLRP3 and Casp1 cleavage (Fig. 6B). FLICA assay was also performed on PBS and α-Syn PFF-injected mouse ventral midbrain sections, followed by double immunostaining for TH and p-S129 α-Syn. A significant increase of the FLICA signal, a marker of Casp1 activity, and p-S129 α-Syn immunostaining, a marker of pathologic α-Syn, was observed within DA neurons of α-Syn PFF-injected mice (Fig. 6C). IMARIS reconstruction of the confocal Z-stack demonstrates that the increased p-S129-α-Syn and increased Casp1 activation occurred within TH positive DA neurons of the α-Syn PFF-injected mice (Fig. 6D). α-Syn PFFs also elicited a statistically significant increase in Casp1 activity within Iba-1 positive microglia (Fig. S7A), suggesting that the α-Syn PFF model elicits both cell-autonomous as well as non-cell-autonomous inflammasome activation pathways. Since the accumulation of PARIS drives mitochondrial deficits observed in this model (Brahmachari *et al.*, 2019), we assessed DA neuron inflammasome activation in α-Syn PFF-injected WT and PARIS deficient mice by immunoblotting for cleaved Casp1 (Fig. 6E) and performing the FLICA assay (followed by TH immunostaining) in ventral midbrain sections (Fig. 6F). Both these assays revealed that PARIS was required for DA neuron inflammasome activation in the mouse α-Syn PFF model.

Casp1$^{-/-}$ mice are protected from DA neuron degeneration in the α-Syn PFF model

To assess whether neuronal inflammasome activation contributes to pathologic α-Syn triggered neurodegeneration of DA neurons, Casp1$^{+/+}$ and Casp1$^{-/-}$ mice were stereotaxically injected with α-Syn PFF and PBS into the dorsal striatum. 6 months later, stereological counting of TH and Nissl-stained neurons revealed a rescue of DA neuron loss in α-Syn PFF-injected Casp1$^{-/-}$ mice when compared to Casp1$^{+/+}$ mice (Fig. 6G and 6H). α-Syn PFF-injected Casp1$^{-/-}$ mice were significantly resistant to behavioral abnormalities in the pole test (Fig. 6I, Video S2) and had preserved forelimb and all-limb strength compared to Casp1$^{+/+}$ mice (Fig. 6J). Immunoblot analysis revealed a significant loss of TH expression in the striatal lysates of α-Syn PFF-injected Casp1$^{+/+}$ mice, accompanied by an increase in oligomeric α-Syn accumulation and pS129-α-Syn levels in the Triton-X insoluble fractions of the ventral midbrain lysates. Casp1$^{-/-}$ mice had significantly improved preservation of TH-expression and reduced oligomeric α-Syn accumulation and p-S129-α-Syn levels (Fig. 6K). These results indicate that pathologic α-Syn leads to the inactivation of parkin, resulting in neuronal NLRP3 inflammasome priming and activation, which is dependent on PARIS. Subsequent Casp-1 activation contributes to the degeneration of DA neurons.

NLRP3 inflammasome activation in human PD postmortem DA neurons

Examination of human postmortem PD SNpc lysates revealed reduction of parkin autoubiquitination, along with a significant upregulation of NLRP3, PARIS and cleaved Casp1 levels, when compared to age-matched controls (Fig. 7A). IHC for TH and NLRP3 in PD brain showed significantly higher levels of NLRP3 within the surviving TH neurons of the SNpc (Fig. 7B). The FLICA assay was performed on fresh-frozen PD and age-matched control ventral midbrain sections, followed by double immunostaining for ASC and TH. DA neurons in the PD brain sections showed upregulated Casp1 activity as well as the formation

of ASC specks (Fig. 7C). We also observed non-DA cells in the PD SNpc positive for ASC specks, as indicated by yellow arrows (FLICA positive DA neurons are indicated with white arrows) in Fig. 7D.

Discussion

The major finding of this paper is that the NLRP3 inflammasome is activated in DA neurons in PD, which contributes to DA neuronal loss. In addition, the absence or inactivation of parkin leads to the priming of the NLRP3 inflammasome via NLRP3 accumulation, since NLRP3 is a parkin polyubiquitination substrate. Parkin loss also activates the NLRP3 inflammasome within DA neurons as a result of the upregulation of another parkin substrate, PARIS. Subsequent activation of the NLRP3 inflammasome effector protease Casp1 leads to the loss of DA neurons.

Inflammasomes are multimeric signaling platforms comprised of a pattern-recognition receptor, the adaptor protein ASC, and Casp1 (Martinon et al., 2002). These complexes were discovered in immune cells and were found to assemble in response to pathogen infection (von Moltke et al., 2013). Their assembly culminates in the autoproteolytic activation of Casp1 and subsequent Casp1-mediated cleavage of pro-cytokines pro-IL-1β and pro-IL18 to their secreted forms (Martinon *et al.*, 2002; Ozoren et al., 2006). Activation of the NLRP3 inflammasome (the best-characterized among the inflammasome subtypes) is a tightly regulated process, requiring two independent steps – (canonical) priming and activation (Lamkanfi and Dixit, 2014). In Alzheimer's disease and PD, the NLRP3 inflammasome contributes to the progression of pathology by assembly and activation in microglia (Gordon *et al.*, 2018; Heneka et al., 2013; Panicker *et al.*, 2019). We show here that the E3 ubiquitin ligase parkin plays a substantial role in inhibiting the priming and activation of the NLRP3 inflammasome within DA neurons. Parkin binds and polyubiquitinates NLRP3, targeting it for proteasomal clearance. In the absence of parkin or upon its inactivation, NLRP3 accumulates in DA neurons leading to inflammasome priming. Unlike in myeloid cells, where inflammogen-mediated NF-κB activation is required for canonical NLRP3 inflammasome priming/NLRP3 induction, the loss of parkin in DA neurons is sufficient to induce inflammasome priming via the accumulation of NLRP3. Activation of the NLRP3 inflammasome occurs in DA neurons through the accumulation of another parkin substrate, PARIS, which leads to mitoROS generation via inhibition of Peroxisome proliferator-activated receptor-gamma coactivator (PGC-1α)-mediated mitochondrial biogenesis (Pirooznia *et al.*, 2022; Pirooznia *et al.*, 2020; Shin *et al.*, 2011; Stevens *et al.*, 2015). The priming and activation of the NLRP3 inflammasome, culminating in Casp1 activation was observed in DA neurons in adult conditional parkin KO mice, hDA neurons lacking PARKIN and in the α-Syn PFF model of DA neuron degeneration. Molecular signatures of this process are evident in human post-mortem DA neurons providing pathophysiologic relevance. Consistent with the idea of neuron-specific inflammasome activation is the observation of neuronal activation of the AIM2 inflammasome in synapse-elimination during neurodevelopment (Lammert *et al.*, 2020) and the observation of expression of NLRP3 in DA neurons (von Herrmann et al., 2020; von Herrmann et al., 2018) as well as the documentation of neuronal activation of Casp1 in pathologic α-Syn models (Ganjam et al., 2019; Wang et al., 2016). Assembly of

the NLRP3 inflammasome complex in PARKIN-deficient hDA neurons did not result in detectable IL-1β or IL-18 secretion, although it did result in increased levels of Gasdermin-D cleavage, suggesting that the neurons might be dying via pyroptotic cell death. Both adult-onset parkin-depleted mouse DA neurons, as well as cultured PARKIN-deficient hDA neurons exhibited NLRP3 upregulation and Casp1 cleavage. Future studies are required to determine whether this parkin-dependent priming of the NLRP3 inflammasome also occurs in microglia as previous studies have implicated parkin deficiency as a contributor to inflammasome activation in immune cells (Mouton-Liger et al., 2018). Although depleting microglia under the settings of adult-onset DA-neuron parkin ablation did not affect neuronal Casp1 activation, glial-neuronal interplay and temporal inflammasome signaling in non-neuronal cells may still contribute to DA neuron death at other time points. Consistent with this notion is the recent observation that STING activation in microglia contributes to the degeneration of DA neurons in the α-Syn PFF model of DA neuron degeneration (Hinkle, 2022). Mitochondrial dysfunction may contribute to pro-inflammatory processes in glia, including the activation of the STING pathway and NLRP3 inflammasome assembly (Lin et al., 2022). In DA neurons, mitochondrial dysfunction may directly lead to neuron dysfunction and death, which may occur *via* pyroptosis. Due to the fact that microglia can express abundant ASC, we cannot rule out microglial ASC speck formation contributes to neurodegeneration in the adult-onset DA neuron parkin depletion model. The temporal dynamics of NLRP3 activation in neurons versus microglial and the relative role of cell autonomous and non-cell autonomous contributions to DA cell death requires further study.

In summary, we present evidence for a novel signaling mechanism of NLRP3 inflammasome priming and activation in DA neurons in PD. We demonstrate that loss of parkin simultaneously primes the NLRP3 inflammasome in DA neurons via accumulation of NLRP3 and activates the NLRP3 inflammasome in DA neurons via upregulation of PARIS. This leads to inflammasome assembly and activation of Casp1 that causes DA neuron loss. Other factors, such as proteostatic stress or alternate parkin substrates may also cross talk and contribute to the priming and activation of the neuronal NLRP3 inflammasome. Our studies indicate that neuronal assembly of the NLRP3 complex contributes to the pathology of this progressive disease. The role of neuronal NLRP3 inflammasome assembly in neurodegeneration indicates that therapeutic strategies targeting inflammasome activation are an important avenue for disease-modifying therapies targeting cell-autonomous cell death mechanisms in PD and potentially other neurodegenerative diseases.

STAR METHODS

RESOURCE AVAILABILITY

Lead Contact—Further information and requests for resources should be directed to and will be fulfilled by the Lead Contact, Ted M. Dawson, M.D., Ph.D. (tdawson@jhmi.edu).

Materials Availability—All biological resources, antibodies, cell lines and model organisms and tools are either available through commercial sources or the corresponding authors. All unique/stable reagents generated in this study are available from the Lead Contact with a completed Materials Transfer Agreement. Further information and requests

for resources and reagents listed in Key Resources Table should be directed to the Lead Contact.

Data and Code Availability

- The data sets generated during the current study are available within the paper or from the corresponding author on reasonable request.
- This paper does not report original code.
- Any additional information required to reanalyze the data reported in this paper is available from the lead contact upon request.

EXPERIMENTAL MODEL AND SUBJECT DETAILS

Animals—C57BL/6 (WT), Nlrp^{3A350VneoR} (NLRP3 knock-in, strain 017969), Nlrp3 deficient mice (strain no.021302), Casp1 deficient (Casp1$^{-/-}$) mice (strain 016621) were obtained from Jackson Laboratories (Bar Harbor, ME). Parkin$^{flx/flx}$ Exon 7 floxed parkin mice were generated previously (Shin *et al.*, 2011; Stevens *et al.*, 2015). We bred Casp1$^{-/-}$ mice with parkin$^{flx/flx}$ mice to obtain Casp1$^{+/-}$/ parkin$^{+/flx}$ mice, which were interbred to obtain Casp1$^{-/-}$ /parkin$^{flx/flx}$ and Casp1$^{+/+}$ /parkin$^{flx/flx}$ littermate control mice. Littermate control mice were used for all experiments. All mice were subjected to adult-onset DA parkin depletion or PBS/ α-Syn PFF treatment at 8–10 weeks of age. Znf746/PARIS deficient mice were generated previously (Brahmachari *et al.*, 2019). All housing, breeding, and procedures were performed according to the NIH Guide for the Care and Use of Experimental Animals and approved by Johns Hopkins University Animal Care and Use Committee. Randomized mixed-gender cohorts were used for all animal experiments. There was no influence or association of sex with our findings.

Human embryonic stem cell (hES) differentiated DA neuron culture—All procedures involving human embryonic stem cells were approved by and conformed to the guidelines of the Johns Hopkins Medicine Institution Review Board and Johns Hopkins University Institutional Stem Cell Research Oversight Committee. H1 human embryonic stem cells (Wi Cell, Madison, WI) were cultured using the standard protocol on inactivated mouse embryonic fibroblasts. hES cells were differentiated into DA neurons using an established protocol (Kriks et al., 2011). Single cells hES cells were cultured on matrigel coated plates at a density of 40,000 cells/cm^2 in SRM media containing growth factors and small molecules including 100 ng/ml FGF8a, 100 ng/ml SHH C25II, 100 nM LDN193189, 10 μM SB431542, 3 μM CHIR99021 and 2 μM Purmorphine for first five days. Cells were maintained for the next six days in neurobasal medium containing B27 minus vitamin A, N2 supplement along with LDN193189 and CHIR99021. Finally, cells were made into single cell suspension and seeded at a density of 400,000/cm^2 onto polyornithine and laminin coated plates in a neurobasal media containing B27 minus Vitamin A, 20 ng/ml BDNF, 20 ng/ml GDNF, 1 ng/ml, 0.2 mM TGFβ ascorbic acid, 0.5 mM cAMP and 10 μM DAPT until maturation (approx. 60 days). The protocol for the generation and characterization of parkin knockout hES cells, as well as CRISPR/Cas9 mediated knockdown of PARIS in the parkin deficient DA neurons is described in detail (Kumar *et al.*, 2020).

Primary microglial cell culture—Microglia were isolated as described in previous publications, with minor modifications (Kam et al., 2018; Panicker *et al.*, 2019). P0 or P1 mice were euthanized, and their brains harvested in ice-cold DMEM/F12 medium. The brains were then gently agitated for 15 min in 0.25% trypsin-EDTA. Trypsinization was stopped by adding DMEM/F12 supplemented with 10% heat-inactivated FBS, 50 U/ml penicillin, 50 μg/ml streptomycin, 2 mM L-glutamine, 100 μM nonessential amino acids, and 2 mM sodium pyruvate. Single-cell suspensions of the cells were then made by trituration and passing the cell-suspension through a 70-μm nylon mesh cell strainer. The cells were then plated out into T75 or T175 flasks. They received a complete medium change at 6 days post culture. Microglial cells were separated 14 days post culture using the EasySep Mouse CD11b Positive Selection Kit II and were allowed to recover for 48 h post separation. The NLRP3 inflammasome was activated by priming the cells with 1 μg/mL LPS for 3 hours, followed by adding 2mM ATP for 45 mins. Supernatants were collected and stored at −80°C.

Post-mortem PD and age-matched control brains—Fresh frozen and sectioned PD and age-matched control SNpc brain sections were obtained from the Division of Neuropathology, Department of Pathology at Johns Hopkins School of Medicine. These were immediately stored at −80 degrees until required. Fresh frozen tissue blocks from the same subjects were provided separately and were utilized for immunoblotting, as described in a subsequent section. The Johns Hopkins Medical Institutions' Joint Committee on Clinical Investigations decided that these studies are exempt from Human Subjects Approval because of Federal Register 46.101 Exemption Number 4. The demographics of the PD brain subjects, as reported in Fig. S1, are as follows: 5/6 subjects were White, 1/6 subjects was American/Alaskan native. In the age-matched control subjects, 5/6 were White, and 1/6 was African American. We did not explore whether sex played a role in the activation of the neuronal inflammasome in human subjects since a large fraction (5/6) of our age-matched control subjects were male.

Methods

Adult-onset DA-neuron specific parkin deletion/NLRP3 inflammasome activation: Parkin$^{flx/flx}$ mice, Casp1$^{-/-}$ /parkin$^{flx/flx}$ and littermate control Casp1$^{+/+}$ / parkin$^{flx/flx}$ mice, or Nlrp3^{A350VneoR} or the NLRP3 mice were deeply anesthetized with a mixture of ketamine (100 mg/kg) and xylazine (10 mg/kg). Conditional DA-neuron knockdown of parkin (in the case of the parkin$^{flx/flx}$ mice) or conditional DA-neuron inflammasome activation (in the case of the Nlrp3^{A350VneoR} mice) was achieved by stereotaxic introduction of an adeno-associated virus serotype 2 (AAV2) vector encoding the GFP fused Cre recombinase (AAV GFP-Cre) into SNpc of 6 to 8 week old mice of the relevant genotype. The AAV GFP-Cre and AAV-GFP constructs were purchased from Vector Biolabs. AAV2-GFP injections served as the appropriate control on the contralateral side. The stereotaxic coordinates, relative to the bregma were (1.3 mm lateral, 3.2 mm caudal, 4.3 mm ventral). The viral titers used for each construct used are as follows: AAV NLRP3-shRNA / AAV PARIS-shRNA: 2X 10^{12} genome copies (GC) /mL (2 μL injected per SNpc), AAV con-shRNA −8.7 X 10^{12} GC /mL (~0.46 μL injected per SNpc), AAV GFP/AAV GFP-Cre - 1 X 10^{13} GC /mL (1 μL injected per SNpc). After each injection

was completed, the needle was maintained in position for 5 mins. Animals were regularly monitored post-surgery. Behavioral tests were performed 3 months post injection. The mice were then euthanized. For biochemical assays, relevant brain regions were dissected out and immediately frozen at −80°C. For histological studies, mice were transcardially perfused with PBS and 4% paraformaldehyde. The brains were then removed, followed by fixation in 4% PFA overnight. The brains were then transferred to a 30% sucrose solution for cryoprotection.

Adult-onset microglia ablation in parkin$^{flx/flx}$ mice: PLX5622 (batch#98636) was obtained from MedChemExpress LLC (NJ, USA) and incorporated into Teklad 2018SX Grain-based Chow Diet (at 1.2 g/kg PLX5622) by Research Diets Inc (NJ, USA). 6–7-week-old parkin$^{flx/flx}$ mice were administered the PLX5622 diet, or the control Teklad 2018SX Grain-based Chow diet, (also supplied by Research Diets Inc) for 20 days. Following this, adult-onset DA-neuron specific parkin deletion was accomplished as described in the previous section. Microglia depletion was assessed via immunoblot and IHC analysis for Iba-1.

Preparation of α-Syn PFFs: Recombinant mouse α-Syn protein was prepared and purified as previously described (Mao et al., 2016). Endotoxin contamination was removed using Toxineraser endotoxin removal kit (Genscript, Piscataway, NJ). α-Syn PFFs were prepared in PBS by constantly agitating α-Syn with a thermomixer (1,000 rpm at 37°C) (Eppendorf, Hamburg, Germany). After 7 days of incubation, the a-syn aggregates were diluted to 0.1 mg/ml with PBS and sonicated for 30 s (0.5 sec pulse on/off) at 10% amplitude (Branson Digital Sonifier, Danbury, CT)

Antibodies: The following antibodies were used: mouse anti-Caspase-1 (Adipogen, AG-20B-0042-C100), mouse anti-NLRP3 (Adipogen, AG-20B-0014-C100), mouse anti-parkin or Prk8 (Cell Signaling, #4211), rabbit anti-parkin (Cell Signaling, #2132), HRP-conjugated mouse anti-β-actin antibody (Sigma-Aldrich, A3854), rabbit anti-TH (Novus, NB300–109), mouse anti-TH (Novus, MAB7566), goat anti-Iba1 (Abcam, ab5076) rabbit anti-Iba1 (Wako, 019–19741), rabbit anti-Iba1 for western blotting (Wako, 016–20001) rabbit anti-ASC (Adipogen, AG-25B-0006-C100), rabbit anti-GFP (Cell Signaling, #2956), mouse anti-HA (Thermo Fisher # 26183–1MG), rabbit anti-GST (Cell Signaling, #2622), mouse anti-FLAG (Sigma Aldrich, F3165), rabbit anti-FLAG (Sigma-Aldrich, F7425), mouse anti-myc (Thermo Fisher, # MA1–980), rabbit anti-myc (Cell Signaling, #5605), HRP-conjugated mouse anti-myc (Cell Signaling, #2040,) rabbit anti-PARIS (Proteintech, 24543–1-AP), rabbit anti-Ub (Novus, NB300–129), rabbit anti-pS129 αSynuclein (Abcam, ab51253), mouse anti-pS129 αSynuclein (Wako, 015–25191), rabbit anti-PINK1 (Cell Signaling, #6946), mouse anti-IL-1β (Cell Signaling #12242), mouse anti TUJ1 (R&D Systems, MAB1195) rabbit anti-alpha tubulin (Cell Signaling, #2144). rabbit anti-Htra2 (Cell Signaling, #2176), rabbit anti-IL-18 (Cell Signaling, #54943), mouse anti-Gasdermin-D (Adipogen, AG-25B-0036-C100), rabbit anti-β-actin-HRP (Cell Signaling, #5125)

Stereotaxic injection of α-Syn PFFs: Two to 3-month-old Casp1$^{-/-}$ and littermate control Casp1$^{+/+}$ mice, or PARIS$^{-/-}$ mice and littermate control PARIS$^{+/+}$ mice were anesthetized

as described in the previous section. α-Syn- PFFs were injected into the striatum (2 μL per hemisphere at 0.4 μL/min). The stereotaxic coordinates, relative to the bregma were anteroposterior (AP) = +0.2 mm, mediolateral (ML) = + 2.0 mm, dorsoventral (DV) = +2.8 mm. An equal volume of PBS was injected as the appropriate control. Post-surgery care was provided as described in the previous section. The mice were euthanized, and tissues collected as described in the previous section.

DAB Immunohistochemistry and Stereological DA neuron counting in the SNpc: Cryopreserved brains were frozen in OCT buffer. A microtome was used to cut 30 μm thick serial coronal sections. These were blocked with 4% goat serum plus 0.2% Triton X-100 in PBS and incubated with an antibody against TH (Novus Biologicals, Littleton, CO, USA). This was followed by incubation with biotin-conjugated anti-rabbit antibody (Vectastain Elite ABC Kit, Vector laboratories, Burlingame, CA, USA). The reaction color was developed using SigmaFast DAB Peroxidase Substrate (Sigma-Aldrich). Sections were counterstained with Nissl stain (0.09% thionin). TH and Nissl-positive neurons in the SNpc were counted using an unbiased stereological method as described previously (Kam *et al.*, 2018; Panicker *et al.*, 2019) using a computer- assisted image analysis system consisting of an Axiophot photomicroscope (Carl Zeiss Vision) equipped with a computer controlled motorized stage (Ludl Electronics), a Hitachi HV C20 camera, and Stereo Investigator software (MicroBright-Field).

In vivo FLICA (Casp1 activity) assay: Fresh frozen human brain sections, live hDA neurons or frozen serial mouse brain sections were assessed for Casp1 activity using the FAM-FLICA Caspase-1 (YVAD) Assay Kit (ImmunoChemistry Technologies, Bloomington, MN). The FLICA reagent is a cell-permeable dye that enters cells and binds to activated Casp1. After FLICA staining, we proceeded to use immunofluorescence for staining in other imaging channels, as described in the subsequent section.

Immunofluorescence analysis: Immunofluorescence was performed on brain sections or cultured hDA neurons as previously described, with a few modifications (Kam *et al.*, 2018; Panicker *et al.*, 2019). Cultured neurons or brain sections were fixed in 4 % paraformadehyde for 18 mins. Coronal brain sections or fixed neurons were blocked in 5% goat or donkey serum with 0.3% Triton X-100 in PBS for 45 mins. This was followed by a second block step using 5% goat or donkey serum within PBS for 15 mins. Primary antibodies were prepared in in 5% goat or donkey serum with 0.1% Triton X-100 in PBS. Primary antibodies included TH (Novus Biologicals and Sigma-Aldrich), pSer129-α-syn (Wako), NLRP3 (Adipogen), ASC (Adipogen), Iba1 (Abcam), GFP (Cell Signaling) and were left on overnight at 4°C. After multiple washes in PBS the following day, Alexa-fluor 488- and 568 or 633 conjugated secondary antibodies (Invitrogen) were used for 1 hr at room temperature. The sections were washed multiple times again in PBS. The VECTASHIELD HardSet Antifade Mounting solution (Vector Laboratories, Burlingame, CA) was used to mount the section or cells. Fluorescent images were acquired by confocal scanning microscopy using the Zeiss LSM 880 Airyscan Microscope (Carl Zeiss). All the images were processed by the Zen software (Carl Zeiss). The selected area in the signal intensity range of the threshold was measured using ImageJ analysis. Imaris software,

available at the Multiphoton Imaging Core at Johns Hopkins School of Medicine was used to analyze Z-stack images. The surface reconstruction wizard in Imaris was used to generate 3D reconstructions of 3 dimensional confocal stacks.

Lysate preparation and immunoblotting: Tissues or cultured cells were homogenized the RIPA lysis buffer comprising 50 mM Tris-HCl (pH 7.4), 150 mM NaCl, 1 mM EDTA, 1% Triton X-100, 0.5% SDS, 0.5% sodium-deoxycholate and 1:100 Protease/Phosphatase Inhibitor Cocktail (Cell Signaling). Post homogenization, samples were rotated at 4°C for 30 min for complete lysis. This homogenate was subsequently centrifuged at 22,000 × g for 35–40 min, and the supernatant was collected for immunoblot. Protein levels were quantified using the BCA Kit and normalized (Pierce, Rockford, IL, USA) with BSA standards. 2x Laemlli Buffer plus β-mercaptoethanol was added to these samples.10–20 μg of total protein lysate was resolved on Novex WedgeWell 4 to 20% or 8–16 % Tris Glycine gels (Thermo Fisher). The proteins were then transferred to nitrocellulose membranes. The membranes were blocked with the Intercept (TBS) Blocking Buffer (LiCor Biosciences). Primary and secondary antibodies were diluted in Intercept Blocking Buffer + 0.1% Tween-20. Washes were done in TBS + 0.1 % Tween. IR-680 or IR-800 conjugated anti-mouse and anti-rabbit (LiCor) antibodies were used for detection, at a dilution of 1:10000. Fluorescent western blots were imaged using the LiCor Odyssey CLx system (LiCor Biosciences) Finally, the membranes were stripped and re-probed with HRP-conjugated β-actin antibody (1:40,000, Sigma-Aldrich). The β-actin bands were visualized by enhanced chemilumescence (Thermo Scientific, IL, USA). Supernatant blots for IL-1β and IL-18 were performed by chloroform-methanol precipitation of the supernatants as described in a previous publication (Kam *et al.*, 2018; Panicker *et al.*, 2019). 400 μl methanol and 100 μl chloroform was added to 400–500 μl of cell supernatants obtained from inflammasome-activated microglia, iCont and PARKIN deficient hDA neurons. The samples were vortexed for 30 s, then centrifuged at 13,000 g for 5 min. After this, we gently removed the aqueous phase using vacuum. The chloroform-methanol precipitated pellets were then dried for 12 min at 55°C. We then added 2X Laemmli buffer and thoroughly vortexed the samples. The lysates were briefly boiled and used for immunoblotting.

In vivo co-immunoprecipitation (Co-IP): Ventral midbrain tissues were suspended in lysis buffer that contained 50 mM Tris-HCl (pH 7.4), 150 mM NaCl, 1 mM EDTA, 1% Triton X-100 and 1:100 Protease/Phosphatase Inhibitor Cocktail (Cell Signaling). Tissues were then homogenized using an automatic homogenizer. They were then incubated on ice for 30 min. This was followed by three freeze-thaw cycles using dry ice and water respectively. The lysates were spun down at 22,000 × g for 35–40 min, and the supernatant was collected for Co-IP. Protein levels were quantified using the BCA Kit and normalized (Pierce, Rockford, IL, USA). 5 % of total lysate was set aside as the input fraction. 2x Laemlli Buffer plus β-mercaptoethanol was added to these samples. 1 mg of total protein was used per Co-IP reaction. 0.5 μg of mouse IgG control (Thermo Fisher) or mouse Parkin (Cell Signaling) antibodies were added. The Co-IP mixtures were rotated overnight at 4°C. 30 μL of Protein G Magnetic Beads (SureBeads, Biorad) were washed and resuspended in the Co-IP buffer, and then added to the lysates for 4 hrs at 4°C. while rotating. The lysates were washed 5 times in the Co-IP buffer using a DynaMag Magnet (Thermo Fisher). After this, 2x Laemlli

Buffer plus β-mercaptoethanol was added to the beads, which were boiled for 5 mins. Co-IP was verified using immunoblotting. We used the rabbit parkin antibody for verifying IP via immunoblot.

Cell culture and transfection of SH-SY5Y cells: SH-SY5Y cells (ATCC, Manassas, VA) were cultured in DMEM containing 10% fetal bovine serum and penicillin/streptomycin at 37°C under 5% CO2. These cells were transfected using the PolyFect reagent (Qiagen) according to manufacturer's instructions.

In-cell co-immunoprecipitation (Co-IP): SH-SY5Y cells were lysed in the Co-IP buffer described previously (in the in vivo Co-IP section). 10–15 % total lysate was set aside as the input fraction. 2x Laemlli Buffer plus β-mercaptoethanol was added to these samples. FLAG-tagged proteins were immunoprecipitated using Anti-FLAG M2 Magnetic Beads (Thermo Fisher) and Myc-tagged proteins were immunoprecipitated using Anti-c-Myc Magnetic Beads (Chromotek) as per manufacturer's instructions. Co-IP was verified using immunoblotting. We prefer to use the rabbit FLAG antibody for assessing immunoprecipitated FLAG-NLRP3.

GST pulldown assay: Recombinant NLRP3 protein (Abcam) was incubated with recombinant GST-parkin or GST alone in GST reaction buffer (250 mM Tris-HCl at pH 7.4, 500 mM Nacl, 25 mM $MgCl_2$, 5 mM dithiothreitol, 0.5 mM EGTA and 20 mM freshly prepared ATP) for 1 hour at 4°C on a rotator. Pierce Glutathione Magnetic Agarose Beads (Thermo Fisher) were then suspended in the GST reaction buffer and then added to the reaction mixture for 1 hour at 4°C on a rotator. The beads were then washed 4 times in reaction buffer using a DynaMag Magnet (Thermo Fisher). 2x Laemlli Buffer plus β-mercaptoethanol was added to these samples, which were then boiled for 5 mins. GST pulldown was verified via immunoblot.

In-cell ubiquitination assay: SH-SY5Y cells were transfected with FLAG-tagged NLRP3 constructs, myc-tagged WT or C431S parkin constructs, HA-tagged WT or KO Ubiquitin constructs for 48 hrs. FLAG-tagged NLRP3 was immunoprecipitated using Anti-FLAG M2 Magnetic Beads (Thermo Fisher) as previously described in the in-cell co-immunoprecipitation section. NLRP3 polyubiquitination was detected using immunoblots for the HA antibody that detected polyubiquitin chains on NLRP3, and also by using the FLAG antibody that detected high molecular weight NLRP3 smears.

TUBE (Tandem Ubiquitin Binding Entities (TUBE) assay: The TUBE assay was performed as described in Seo et al., (Seo *et al.,* 2021), with some modifications- hDA neurons or mouse ventral midbrain tissues were lysed in buffer that contained 50 mM Tris-HCl (pH 7.4), 150 mM NaCl, 1 mM EDTA, 1% Triton X-100, 100 mM n-ethylmaleimide (NEM) and 1:100 Protease/Phosphatase Inhibitor Cocktail (Cell Signaling). Polyubiquitinated proteins were pulled down using the pan selective, poly-ubiquitin binding magnetic TUBE (UM411M, Life Sensor Technologies). Lysates were then washed thrice in lysis buffer before elution of the polyubiquitinated proteins as per the manufacturer's instructions. The levels of endogenous and polyubiquitinated NLRP3 in input or TUBE fractions respectively were assessed via immunoblot analysis as previously described.

In-vitro ubiquitination assay: A modified version of a previously established protocol (Lee et al., 2017) was employed. The ubiquitination reaction mixture contained 40 ng of UBE1 (E1, Boston Biochem), 200 ng UbcH7 (E2, Boston Biochem) and 1 μg His-Ub (Boston Biochem). To this, we added 500 ng of WT or C431S parkin, 500 ng of wild-type or kinase dead TC PINK1 (Boston Biochem). 100 ng of recombinant NLRP3 (Abcam) was added as the substrate. The final reaction buffer contained 50 mM Tris at pH 7.4, 100 mM NaCl. 5 mM $MgCl_2$, 1 mM dithiothreitol, 0.1 mM EGTA and 4 mM freshly prepared ATP. The reaction mixture was agitated at 450 RPM at 37 °C for 40 min. 5x Laemlli Buffer was added. The reaction mixture was then boiled for 5 mins and subjected to SDS-PAGE and Immunoblot analysis. Polyubiquitination of NLRP3 was detected using the anti-NLRP3 antibody. High molecular weight smearing indicated NLRP3 polyubiquitination. Parkin autoubiquitination was detected using the anti-parkin antibody.

Cycloheximide (CHX) chase assay: SH-SY5Y cells were transiently transfected with FLAG-tagged NLRP3 with or without WT parkin or C431S parkin. Cyclohexamide (CHX, 100 μg/ml) was added and time dependent decline in FLAG-NLRP3 level was assessed using immunoblots. Additionally, iCont and PARKIN-deficient hDA neurons were treated with CHX (100 μg/ml), and endogenous NLRP3 levels were assessed using immunoblots. In the proteasome inhibition experiment, the CHX chase assay was performed on SH-SY5Y cells that were transiently transfected with FLAG-tagged NLRP3 with or without WT parkin, that also received a pre-treatment of MG-132 (10 μM) to inhibit the proteasome. Clearance of NLRP3 was assessed via immunoblotting.

MitoROS production assay: MitoROS production in iCont, PARKIN deficient, and PARKIN deficient +PARIS KD hDA neurons was assessed using the MitoSOX Red reagent (Thermo Fisher). 2 μM MitoSOX reagent staining was performed in live DA neurons for 10 mins at 37°C. Following this, the cells were fixed in 4 % paraformaldehyde and counterstained with TH as previously described.

DSS-crosslinking (ASC oligomerization) assay: Cultured iCont, PARKIN deficient, and PARKIN deficient +PARIS KD hDA neurons were lysed in 0.5 mL lysis buffer that contained 20 mM HEPES-KOH at pH 7.5, 150 mM KCl, 1% Nonidet P-40, 0.1 mM phenylmethylsulfonyl fluoride (PMSF) and 1:100 Protease/Phosphatase Inhibitor Cocktail (Cell Signaling). Cells were sheared 10 times through a 21-gauge needle. Cell lysates were then spun down at 6000 rpm for 15 mins at 4°C. Supernatants were removed and their protein concentration assessed using the BCA assay as previously described. The cell-pellets were suspended in 500 μL PBS at pH 7.4. 2 mM disuccinimidyl suberate (DSS) (Thermo Fisher) was then added from a freshly prepared 100 mM DSS stock solution. The reaction mixtures were then gently rotated for 40 mins at room temperature. Samples were spun down at 6000 rpm for 15 mins at 4°C. The cross-linking was quenched by adding 2x Laemlli buffer. The reaction mixture was then boiled for 5 mins, and oligomerization of ASC was assessed using immunoblots. The non-DSS fraction was also assessed for endogenous, non-oligomerized ASC via immunoblots.

Cell death assay: Cultured iCont, PARKIN deficient, and PARKIN deficient +Casp1 KD/MCC-950 hDA neurons were assessed for cell death using propidium iodide (PI) staining. Percent of cell death was determined by staining with 7 mM Hoechst 33342 and 2 mM PI (Invitrogen). Images were taken and counted by a Zeiss microscope equipped with automated computer assisted software (Axiovision 4.6, Carl Zeiss, Dublin, CA).

CRISPR Cas9 knockdown of Casp1: Guide RNAs targeting the 5'UTR and Exon 2 of Casp1 were designed using an online tool (http://crispor.tefor.net/). These guide RNAs were cloned into the LentiCRISPR backbone vector. Lentiviruses packaged with gRNA of interest were validated in SH-SY5Y cells. The Exon-2 gRNA was selected. This was cloned into the LentiCRISPR backbone vector and designated as LV-CRISPR Casp1. The Lentivirus encoding the Casp1 (Exon-2) gRNA (LV-CRISPR Casp1) was used to transduce iCont and PARKIN deficient cultured hDA neurons for 5 days. Cell lysates were prepared as aforementioned, and Casp1 knockdown was confirmed via immunoblot.

Quantitative PCR: Total RNA was isolated from homogenized striatal tissues with TRIzol Reagent (Invitrogen, Waltham, MA) and measured with a NanoDrop 2000 spectrophotomer (Biotek, Winooski, WT). Total RNA (1 ug) was reverse-transcribed to cDNA with the High-Capacity cDNA Reverse Transcription Kit (Applied Biosystems, Waltham, MA) for quantitative RT-PCR (qPCR) with a Viia7 Real-Time PCR System (Applied Biosystems) using SYBR Green Master Mix (Applied Biosystems). Relative gene expression was quantified after normalizing to β-actin expression using the comparative cycle threshold method. Primer sequences used are listed in Supplementary Table 3.

Behavioral tests:

Amphetamine-induced stereotypic rotation: 3 months post intranigral delivery of the AAV-GFP or AAV-GFP Cre constructs, the mice were injected intraperitonially with 5 mg/kg body weight Amphetamine (Sigma-Aldrich). They were placed into cylinders of ~ 20 cm diameter and monitored for 30 min. The behavior of mice was recorded for at least 5 min between 20- and 30-min following amphetamine administration. Full body ipsilateral rotations (clockwise) were counted for each mouse from the video recordings. Investigators performing the assay and recording videos were blinded to mouse genotypes and treatment groups.

Pole test: A metal rod (75 cm long with and 9 mm in diameter) wrapped with bandage gauze was used as the pole. Mice were trained on the pole for two consecutive days before the day of the final pole test. Each training session consisted of three test trials. Mice were placed 7.5 cm from the top of the pole with the snout pointing upwards. The time taken by the mouse to turn and total time to reach the base of the pole were recorded. The end of test was defined by placement of all 4 paws on the base. The maximum cutoff time to stop the test and recording was 60 s. After each trial, the pole was cleaned with 70% ethanol. Investigators performing the assays were blind to genotypes or treatment condition and randomly allocated to groups.

Grip strength test: Grip strength was assayed by determining the maximal peak force developed by the mice using a grip-strength meter (Bioseb, USA). Mice were placed onto a metal grid to grasp with either forelimb or both limbs that were recorded as 'forelimb' and 'fore and hindlimb', respectively. Their tails were gently pulled, and the force applied to the grid before the mice lose their grip was recorded as the peak tension displayed in grams (g).

QUANTIFICATION AND STATISTICAL ANALYSIS

Statistical analysis—Data and statistical analyses were performed using Prism 6.0 (GraphPad Software). The criteria for significance was: ns (not significant) $p > 0.05$, *$p < 0.05$, **$p < 0.01$, ***$p < 0.001$. Differences in means between 2 groups were analyzed using unpaired two-tailed Student's T-test. For more than 2 groups, a one-way ANOVA (with Tukey's post hoc correction for multiple comparisons) was used. For mixed groups, a two-way ANOVA (with Tukey's post hoc correction for multiple comparisons) was used. Graph bars indicate mean, and error bars indicate standard error (SEM) or standard deviation (SD), as indicated. Sample sizes were chosen based on previous publications from our group as well as other articles in the literature. For each in vivo experiment, an "n" represents a separate animal. For in vitro experiments, each "n" represents a separate, independent experiment. The value of each n can be found in the Figure legends.

Supplementary Material

Refer to Web version on PubMed Central for supplementary material.

Acknowledgements

This work was supported by the JPB Foundation and the Farmers Family Foundation Parkinson's Research Initiative and NIH NINDS NS38377. N.P. was supported by a postdoctoral fellowship from the Maryland Stem Cell Research Fund 2017-MSCRFF-3838 and is currently supported by a Pathway to Independence grant from the NIA NIH K99AG066862. X. M. was supported by Parkinson's Foundation, PF-JFA-1933, Maryland Stem Cell Research Fund 2019-MSCRFD-4292, NIA NIH K01 AG056841, and NIH NINDS R01 NS107318. Full-length and truncated FLAG-tagged NLRP3 constructs were obtained from Addgene. The Multiphoton Imaging (MPI) Core in the Department of Neuroscience was used for access to workstations containing the IMARIS software, funded by NINDS Core Center Grant (P30 NS050274). T.M.D. is the Leonard and Madlyn Abramson Professor in Neurodegenerative Diseases. JTH receives stipend support through the Medical Scientist Training Program at Johns Hopkins University (NIH/NIGMS T32GM136577) and through a predoctoral NRSA (NIH/NIA F30AG067643). The authors acknowledge the joint participation by the Adrienne Helis Malvin Medical Research Foundation and the Diana Helis Henry Medical Research Foundation through its direct engagement in the continuous active conduct of medical research in conjunction with The Johns Hopkins Hospital and the Johns Hopkins University School of Medicine and the Foundation's Parkinson's Disease Programs M-1, M2, H-2014.

References

Brahmachari S, Lee S, Kim S, Yuan C, Karuppagounder SS, Ge P, Shi R, Kim EJ, Liu A, Kim D, et al. (2019). Parkin interacting substrate zinc finger protein 746 is a pathological mediator in Parkinson's disease. Brain 142, 2380–2401. 10.1093/brain/awz172. [PubMed: 31237944]

Brydges SD, Mueller JL, McGeough MD, Pena CA, Misaghi A, Gandhi C, Putnam CD, Boyle DL, Firestein GS, Horner AA, et al. (2009). Inflammasome-mediated disease animal models reveal roles for innate but not adaptive immunity. Immunity 30, 875–887. 10.1016/j.immuni.2009.05.005. [PubMed: 19501000]

Dauer W, and Przedborski S (2003). Parkinson's disease: mechanisms and models. Neuron 39, 889–909. 10.1016/s0896-6273(03)00568-3. [PubMed: 12971891]

Di Maio R, Barrett PJ, Hoffman EK, Barrett CW, Zharikov A, Borah A, Hu X, McCoy J, Chu CT, Burton EA, et al. (2016). alpha-Synuclein binds to TOM20 and inhibits mitochondrial protein import in Parkinson's disease. Sci Transl Med 8, 342ra378. 10.1126/scitranslmed.aaf3634.

Exner N, Lutz AK, Haass C, and Winklhofer KF (2012). Mitochondrial dysfunction in Parkinson's disease: molecular mechanisms and pathophysiological consequences. EMBO J 31, 3038–3062. 10.1038/emboj.2012.170. [PubMed: 22735187]

Ganjam GK, Bolte K, Matschke LA, Neitemeier S, Dolga AM, Hollerhage M, Hoglinger GU, Adamczyk A, Decher N, Oertel WH, and Culmsee C (2019). Mitochondrial damage by alpha-synuclein causes cell death in human dopaminergic neurons. Cell Death Dis 10, 865. 10.1038/s41419-019-2091-2. [PubMed: 31727879]

Ge P, Dawson VL, and Dawson TM (2020). PINK1 and Parkin mitochondrial quality control: a source of regional vulnerability in Parkinson's disease. Mol Neurodegener 15, 20. 10.1186/s13024-020-00367-7. [PubMed: 32169097]

Gordon R, Albornoz EA, Christie DC, Langley MR, Kumar V, Mantovani S, Robertson AAB, Butler MS, Rowe DB, O'Neill LA, et al. (2018). Inflammasome inhibition prevents alpha-synuclein pathology and dopaminergic neurodegeneration in mice. Sci Transl Med 10. 10.1126/scitranslmed.aah4066.

Henderson MX, Cornblath EJ, Darwich A, Zhang B, Brown H, Gathagan RJ, Sandler RM, Bassett DS, Trojanowski JQ, and Lee VMY (2019). Spread of alpha-synuclein pathology through the brain connectome is modulated by selective vulnerability and predicted by network analysis. Nat Neurosci 22, 1248–1257. 10.1038/s41593-019-0457-5. [PubMed: 31346295]

Heneka MT, Kummer MP, Stutz A, Delekate A, Schwartz S, Vieira-Saecker A, Griep A, Axt D, Remus A, Tzeng TC, et al. (2013). NLRP3 is activated in Alzheimer's disease and contributes to pathology in APP/PS1 mice. Nature 493, 674–678. 10.1038/nature11729. [PubMed: 23254930]

Hinkle JTP, J.; Panicker N; Karuppagounder SS; Biswas D; Belingon B; Chen R; Brahmachari S; Pletnikova O; Troncoso JC; Dawson VL; Dawson TM (2022). STING mediates neurodegeneration and neuroinflammation in nigrostriatal α-synucleinopathy. Proc Natl Acad Sci U S A 119 (15) e2118819119. 10.1073/pnas.2118819119. [PubMed: 35394877]

Jo A, Lee Y, Kam TI, Kang SU, Neifert S, Karuppagounder SS, Khang R, Kang H, Park H, Chou SC, et al. (2021). PARIS farnesylation prevents neurodegeneration in models of Parkinson's disease. Sci Transl Med 13. 10.1126/scitranslmed.aax8891.

Kam TI, Mao X, Park H, Chou SC, Karuppagounder SS, Umanah GE, Yun SP, Brahmachari S, Panicker N, Chen R, et al. (2018). Poly(ADP-ribose) drives pathologic alpha-synuclein neurodegeneration in Parkinson's disease. Science 362. 10.1126/science.aat8407.

Kane LA, Lazarou M, Fogel AI, Li Y, Yamano K, Sarraf SA, Banerjee S, and Youle RJ (2014). PINK1 phosphorylates ubiquitin to activate Parkin E3 ubiquitin ligase activity. J Cell Biol 205, 143–153. 10.1083/jcb.201402104. [PubMed: 24751536]

Kitada T, Asakawa S, Hattori N, Matsumine H, Yamamura Y, Minoshima S, Yokochi M, Mizuno Y, and Shimizu N (1998). Mutations in the parkin gene cause autosomal recessive juvenile parkinsonism. Nature 392, 605–608. 10.1038/33416. [PubMed: 9560156]

Kriks S, Shim JW, Piao J, Ganat YM, Wakeman DR, Xie Z, Carrillo-Reid L, Auyeung G, Antonacci C, Buch A, et al. (2011). Dopamine neurons derived from human ES cells efficiently engraft in animal models of Parkinson's disease. Nature 480, 547–551. 10.1038/nature10648. [PubMed: 22056989]

Kumar M, Acevedo-Cintron J, Jhaldiyal A, Wang H, Andrabi SA, Eacker S, Karuppagounder SS, Brahmachari S, Chen R, Kim H, et al. (2020). Defects in Mitochondrial Biogenesis Drive Mitochondrial Alterations in PARKIN-Deficient Human Dopamine Neurons. Stem Cell Reports 15, 629–645. 10.1016/j.stemcr.2020.07.013. [PubMed: 32795422]

Lamkanfi M, and Dixit VM (2014). Mechanisms and functions of inflammasomes. Cell 157, 1013–1022. 10.1016/j.cell.2014.04.007. [PubMed: 24855941]

Lammert CR, Frost EL, Bellinger CE, Bolte AC, McKee CA, Hurt ME, Paysour MJ, Ennerfelt HE, and Lukens JR (2020). AIM2 inflammasome surveillance of DNA damage shapes neurodevelopment. Nature 580, 647–652. 10.1038/s41586-020-2174-3. [PubMed: 32350463]

Lee Y, Stevens DA, Kang SU, Jiang H, Lee YI, Ko HS, Scarffe LA, Umanah GE, Kang H, Ham S, et al. (2017). PINK1 Primes Parkin-Mediated Ubiquitination of PARIS in Dopaminergic Neuronal Survival. Cell Rep 18, 918–932. 10.1016/j.celrep.2016.12.090. [PubMed: 28122242]

Lin MM, Liu N, Qin ZH, and Wang Y (2022). Mitochondrial-derived damage-associated molecular patterns amplify neuroinflammation in neurodegenerative diseases. Acta Pharmacol Sin. 10.1038/s41401-022-00879-6.

Luk KC, Kehm V, Carroll J, Zhang B, O'Brien P, Trojanowski JQ, and Lee VM (2012). Pathological alpha-synuclein transmission initiates Parkinson-like neurodegeneration in nontransgenic mice. Science 338, 949–953. 10.1126/science.1227157. [PubMed: 23161999]

Mao X, Ou MT, Karuppagounder SS, Kam TI, Yin X, Xiong Y, Ge P, Umanah GE, Brahmachari S, Shin JH, et al. (2016). Pathological alpha-synuclein transmission initiated by binding lymphocyte-activation gene 3. Science 353. 10.1126/science.aah3374.

Martinon F, Burns K, and Tschopp J (2002). The inflammasome: a molecular platform triggering activation of inflammatory caspases and processing of proIL-beta. Mol Cell 10, 417–426. 10.1016/s1097-2765(02)00599-3. [PubMed: 12191486]

Moon HE, and Paek SH (2015). Mitochondrial Dysfunction in Parkinson's Disease. Exp Neurobiol 24, 103–116. 10.5607/en.2015.24.2.103. [PubMed: 26113789]

Mouton-Liger F, Rosazza T, Sepulveda-Diaz J, Ieang A, Hassoun SM, Claire E, Mangone G, Brice A, Michel PP, Corvol JC, and Corti O (2018). Parkin deficiency modulates NLRP3 inflammasome activation by attenuating an A20-dependent negative feedback loop. Glia 66, 1736–1751. 10.1002/glia.23337. [PubMed: 29665074]

Ozoren N, Masumoto J, Franchi L, Kanneganti TD, Body-Malapel M, Erturk I, Jagirdar R, Zhu L, Inohara N, Bertin J, et al. (2006). Distinct roles of TLR2 and the adaptor ASC in IL-1beta/IL-18 secretion in response to Listeria monocytogenes. J Immunol 176, 4337–4342. 10.4049/jimmunol.176.7.4337. [PubMed: 16547271]

Panicker N, Sarkar S, Harischandra DS, Neal M, Kam TI, Jin H, Saminathan H, Langley M, Charli A, Samidurai M, et al. (2019). Fyn kinase regulates misfolded alpha-synuclein uptake and NLRP3 inflammasome activation in microglia. J Exp Med 216, 1411–1430. 10.1084/jem.20182191. [PubMed: 31036561]

Pirooznia SK, Rosenthal LS, Dawson VL, and Dawson TM (2021). Parkinson Disease: Translating Insights from Molecular Mechanisms to Neuroprotection. Pharmacol Rev 73, 33–97. 10.1124/pharmrev.120.000189. [PubMed: 34663684]

Pirooznia SK, Wang H, Panicker N, Kumar M, Neifert S, Dar MA, Lau E, Kang BG, Redding-Ochoa J, Troncoso JC, et al. (2022). Deubiquitinase CYLD acts as a negative regulator of dopamine neuron survival in Parkinson's disease. Sci Adv 8, eabh1824. 10.1126/sciadv.abh1824. [PubMed: 35363524]

Pirooznia SK, Yuan C, Khan MR, Karuppagounder SS, Wang L, Xiong Y, Kang SU, Lee Y, Dawson VL, and Dawson TM (2020). PARIS induced defects in mitochondrial biogenesis drive dopamine neuron loss under conditions of parkin or PINK1 deficiency. Mol Neurodegener 15, 17. 10.1186/s13024-020-00363-x. [PubMed: 32138754]

Sanjana NE, Shalem O, and Zhang F (2014). Improved vectors and genome-wide libraries for CRISPR screening. Nat Methods 11, 783–784. 10.1038/nmeth.3047. [PubMed: 25075903]

Savitt JM, Dawson VL, and Dawson TM (2006). Diagnosis and treatment of Parkinson disease: molecules to medicine. J Clin Invest 116, 1744–1754. 10.1172/JCI29178. [PubMed: 16823471]

Scarffe LA, Stevens DA, Dawson VL, and Dawson TM (2014). Parkin and PINK1: much more than mitophagy. Trends Neurosci 37, 315–324. 10.1016/j.tins.2014.03.004. [PubMed: 24735649]

Seo BA, Kim D, Hwang H, Kim MS, Ma SX, Kwon SH, Kweon SH, Wang H, Yoo JM, Choi S, et al. (2021). TRIP12 ubiquitination of glucocerebrosidase contributes to neurodegeneration in Parkinson's disease. Neuron 109, 3758–3774 e3711. 10.1016/j.neuron.2021.09.031. [PubMed: 34644545]

Shi H, Wang Y, Li X, Zhan X, Tang M, Fina M, Su L, Pratt D, Bu CH, Hildebrand S, et al. (2016). NLRP3 activation and mitosis are mutually exclusive events coordinated by NEK7, a new inflammasome component. Nat Immunol 17, 250–258. 10.1038/ni.3333. [PubMed: 26642356]

Shin JH, Ko HS, Kang H, Lee Y, Lee YI, Pletinkova O, Troconso JC, Dawson VL, and Dawson TM (2011). PARIS (ZNF746) repression of PGC-1alpha contributes to neurodegeneration in Parkinson's disease. Cell 144, 689–702. 10.1016/j.cell.2011.02.010. [PubMed: 21376232]

Stevens DA, Lee Y, Kang HC, Lee BD, Lee YI, Bower A, Jiang H, Kang SU, Andrabi SA, Dawson VL, et al. (2015). Parkin loss leads to PARIS-dependent declines in mitochondrial mass and respiration. Proc Natl Acad Sci U S A 112, 11696–11701. 10.1073/pnas.1500624112. [PubMed: 26324925]

Swanson KV, Deng M, and Ting JP (2019). The NLRP3 inflammasome: molecular activation and regulation to therapeutics. Nat Rev Immunol 19, 477–489. 10.1038/s41577-019-0165-0. [PubMed: 31036962]

Turrens JF (2003). Mitochondrial formation of reactive oxygen species. J Physiol 552, 335–344. 10.1113/jphysiol.2003.049478. [PubMed: 14561818]

von Herrmann KM, Anderson FL, Martinez EM, Young AL, and Havrda MC (2020). Slc6a3-dependent expression of a CAPS-associated Nlrp3 allele results in progressive behavioral abnormalities and neuroinflammation in aging mice. J Neuroinflammation 17, 213. 10.1186/s12974-020-01866-6. [PubMed: 32680528]

von Herrmann KM, Salas LA, Martinez EM, Young AL, Howard JM, Feldman MS, Christensen BC, Wilkins OM, Lee SL, Hickey WF, and Havrda MC (2018). NLRP3 expression in mesencephalic neurons and characterization of a rare NLRP3 polymorphism associated with decreased risk of Parkinson's disease. NPJ Parkinsons Dis 4, 24. 10.1038/s41531-018-0061-5. [PubMed: 30131971]

von Moltke J, Ayres JS, Kofoed EM, Chavarria-Smith J, and Vance RE (2013). Recognition of bacteria by inflammasomes. Annu Rev Immunol 31, 73–106. 10.1146/annurev-immunol-032712-095944. [PubMed: 23215645]

Wang W, Nguyen LT, Burlak C, Chegini F, Guo F, Chataway T, Ju S, Fisher OS, Miller DW, Datta D, et al. (2016). Caspase-1 causes truncation and aggregation of the Parkinson's disease-associated protein alpha-synuclein. Proc Natl Acad Sci U S A 113, 9587–9592. 10.1073/pnas.1610099113. [PubMed: 27482083]

Wauer T, and Komander D (2013). Structure of the human Parkin ligase domain in an autoinhibited state. EMBO J 32, 2099–2112. 10.1038/emboj.2013.125. [PubMed: 23727886]

Woodroof HI, Pogson JH, Begley M, Cantley LC, Deak M, Campbell DG, van Aalten DM, Whitworth AJ, Alessi DR, and Muqit MM (2011). Discovery of catalytically active orthologues of the Parkinson's disease kinase PINK1: analysis of substrate specificity and impact of mutations. Open Biol 1, 110012. 10.1098/rsob.110012. [PubMed: 22645651]

Zhou R, Yazdi AS, Menu P, and Tschopp J (2011). A role for mitochondria in NLRP3 inflammasome activation. Nature 469, 221–225. 10.1038/nature09663. [PubMed: 21124315]

Highlights

- NLRP3 is a parkin polyubiquitination substrate
- Loss of parkin primes and activates the NLRP3 inflammasome in dopamine neurons
- Accumulation of PARIS due to loss of parkin drives NLRP3 inflammasome activation
- Inhibiting neuronal NLRP3 inflammasome assembly prevents neurodegeneration in PD

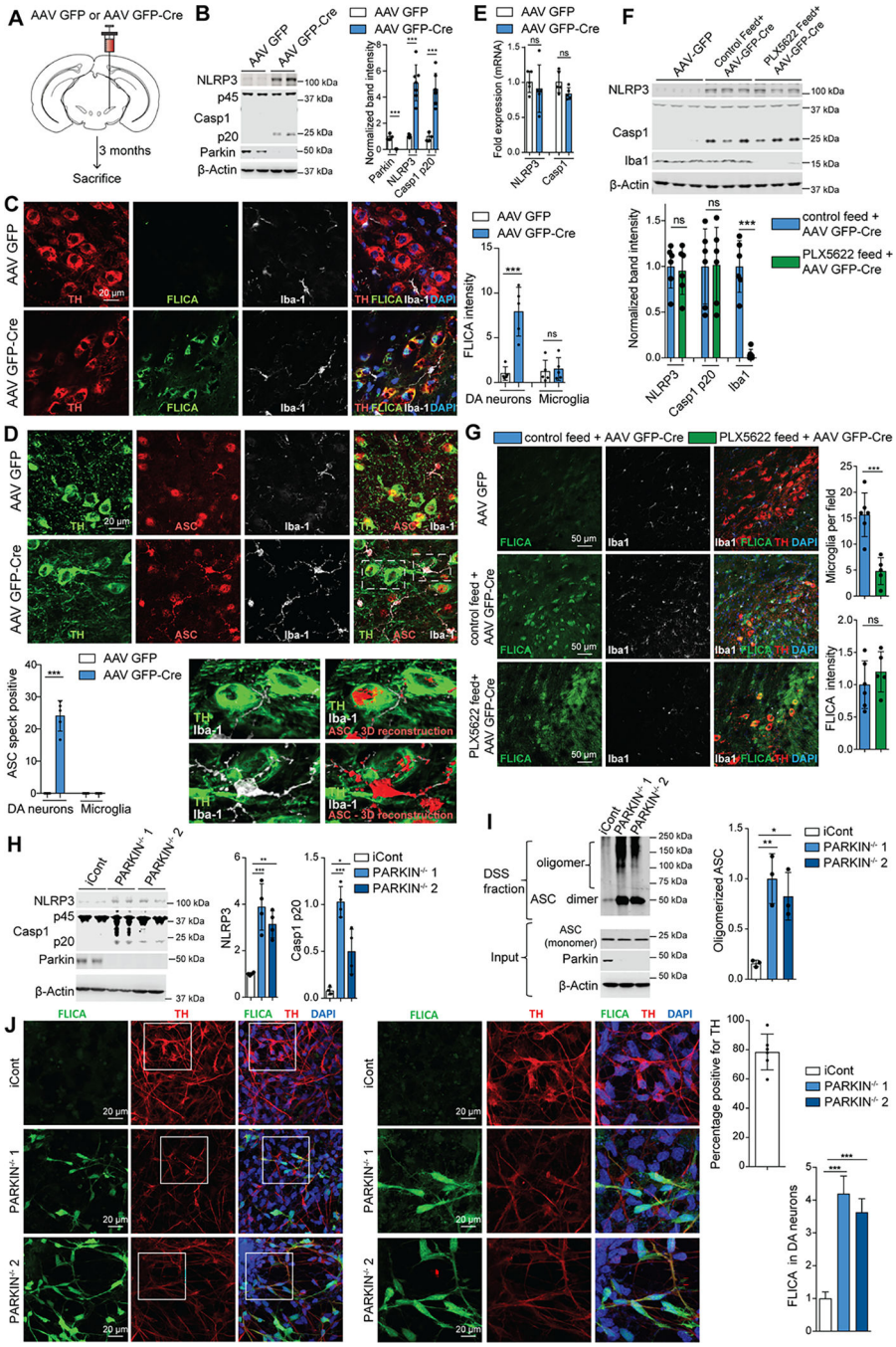

Figure 1: DA neuron specific parkin deletion spontaneously activates the neuronal NLRP3 inflammasome.

A, Schematic of the AAV GFP- or AAV GFP-Cre-injection model in parkin$^{flx/flx}$ mice. **B,** Adult-onset parkin ablation in SNpc DA neurons was sufficient to induce NLRP3 induction as well as Casp1 cleavage, as verified by immunoblot analysis of AAV GFP-and AAV GFP-Cre-injected parkin$^{flx/flx}$ ventral midbrain lysates. Bars represent mean ± s.e.m. n=7). **C,** Representative IHC showing upregulated Casp1 activity, assayed using FLICA staining, in TH positive DA neurons of the SNpc, not Iba-1 positive microglia in AAV GFP-Cre-injected

parkin$^{flx/flx}$ mice. Bars represent mean ± s.e.m (n=5). **D,** Representative IHC showing ASC speck formation within TH positive SNpc DA neurons, but not within Iba-1 positive microglia in AAV GFP-Cre-injected parkin$^{flx/flx}$ mice. Bars represent mean ± s.e.m (n=5). **E,** q-RT PCR shows unchanged NLRP3 and Casp1 mRNA levels in AAV GFP- or AAV GFP-Cre-injected parkin$^{flx/flx}$ mouse ventral midbrain tissues. Bars represent mean ± s.e.m. (n=5) **F,** Representative immunoblots showing that microglia depletion *in vivo* does not affect loss of parkin-mediated NLRP3 induction and Casp1 cleavage. Bars represent mean ± s.e.m. (n=6). **G,** Representative IHC showing no change in DA neuron FLICA activity following microglia depletion in adult-onset DA neuron parkin ablated mouse brains. Bars represent mean ± s.e.m. (n=6). **H,** Representative immunoblot showing increased NLRP3 and cleaved Casp1 in PARKIN deficient hDA neurons when compared to iCont DA neurons. Bars represent mean ± s.e.m. (n=4). **I,** Increased ASC oligomerization in PARKIN deficient hDA neurons when compared to iCont DA neurons, as verified by DSS-crosslinking assay. Bars represent mean ± s.e.m. (n=3). **J,** Representative Immunofluorescence images showing upregulated Casp1 activity, assayed using FLICA staining in PARKIN deficient hDA neurons. Bars represent mean ± s.e.m (n=7).

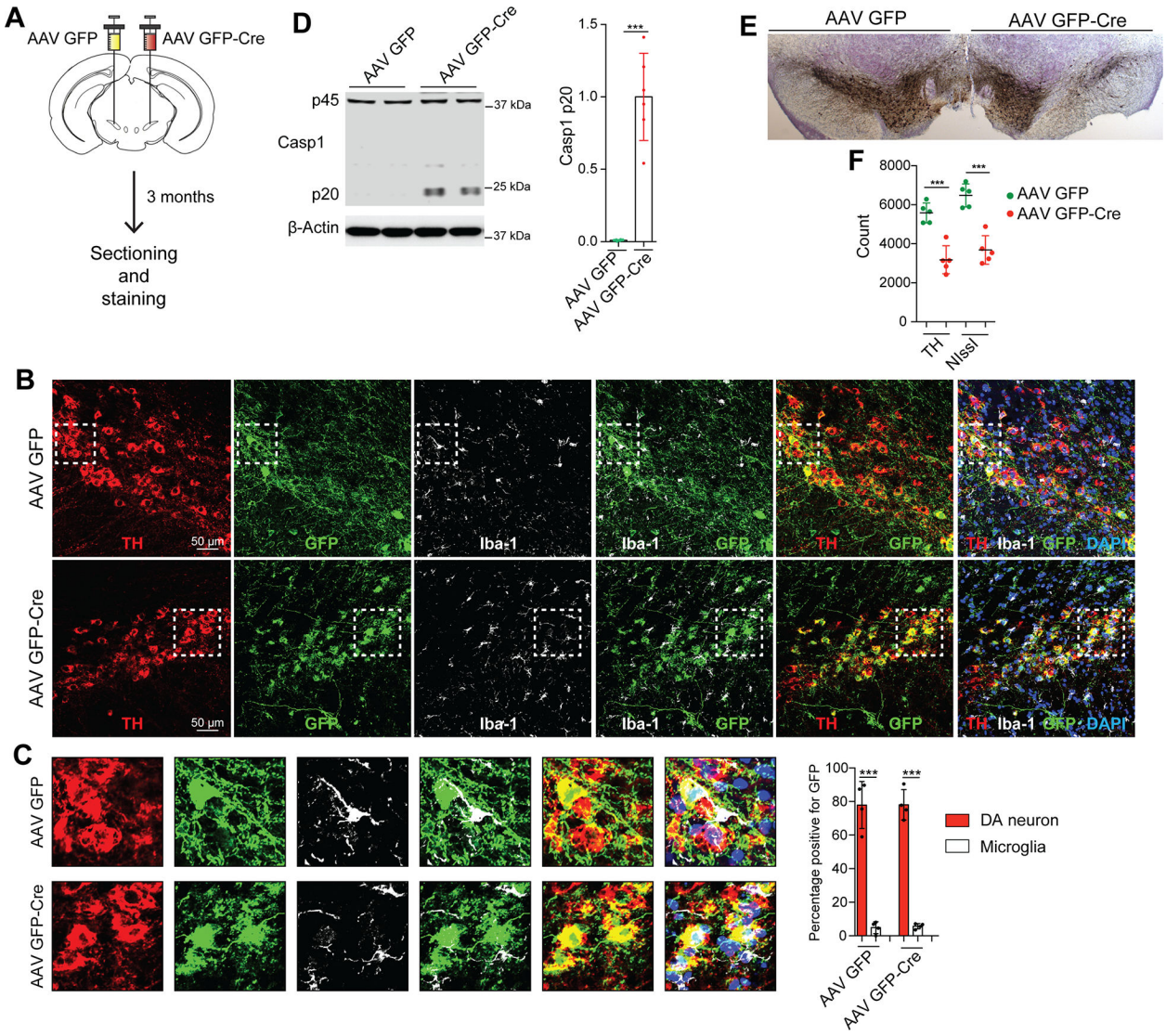

Figure 2: SNpc DA neuron specific NLRP3 inflammasome activation is sufficient to drive DA neuron death.

A, Schematic of the bilateral AAV GFP- and AAV GFP-Cre-injection model in NLRP3^{A350V} mice. **B,** Verification of SNpc DA neuron targeting of AAV GFP- and AAV GFP-Cre-injected NLRP3^{A350V} mice *via* triple staining with TH, GFP, and Iba-1. Bars represent mean ± s.e.m. (n=4). **C,** Higher magnification image showing GFP expression in TH positive DA neurons, not Iba-1 positive microglia. **D,** Representative immunoblot showing increased inflammasome activation in AAV GFP-Cre-injected ventral midbrain lysates of NLRP3^{A350V} mice. Bars represent mean ± s.e.m. (n=6). **E,** Representative ventral midbrain section of NLRP3^{A350V} mouse bilaterally injected in the SNpc with AAV GFP and AAV GFP-Cre stained 3 months post injection with TH and Nissl. **F,** Stereological counting of TH and Nissl positive cells in the SNpc of NLRP3^{A350V} mice subjected to aforementioned-bilateral injection model, showing loss of SNpc DA neurons mediated by SNpc DA neuron specific inflammasome activation. Bars represent mean ± s.e.m. (n=5).

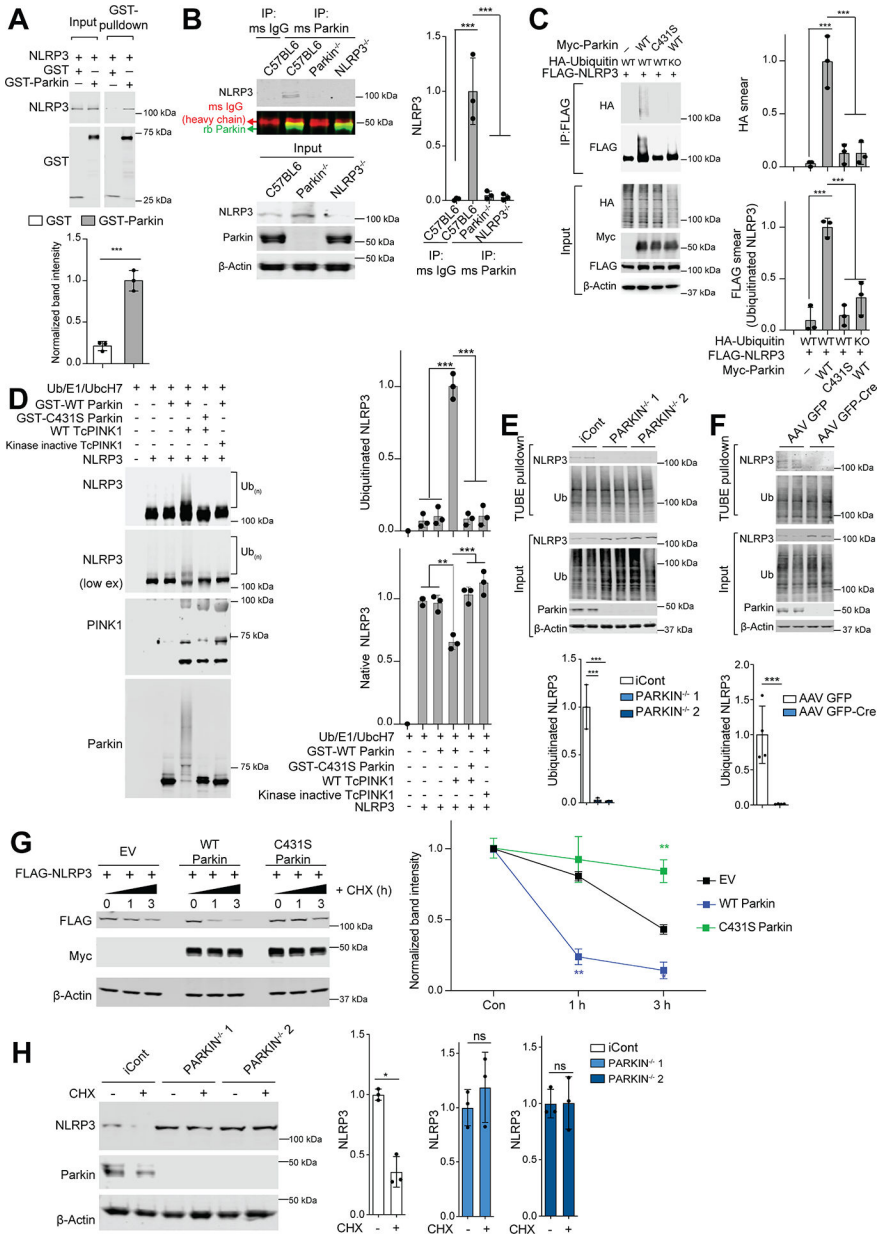

Figure 3: NLRP3 is a parkin polyubiquitination substrate.

A, GST pull-down assay demonstrating direct interaction of recombinant NLRP3 and parkin proteins. Bars represent mean ± s.e.m. (n=3). **B,** Co-immunoprecipitation of parkin and NLRP3 in WT (C57BL6), but not parkin or NLRP3 deficient mouse ventral midbrain lysates. Bars represent mean ± s.e.m. (n=3). **C,** Myc-tagged WT parkin, but not C431S inactive-mutant parkin ubiquitinates FLAG-NLRP3, as evidenced by an in-cell ubiquitination assay. HA-tagged WT Ub, but not (lysine-mutated) KO Ub can be incorporated into polyubiquitinated NLRP3 chains. Bars represent mean ± s.e.m. (n=3). **D,** *In vitro* ubiquitination assay shows that Tc PINK1-activated WT, but not C431S recombinant parkin could ubiquitinate NLRP3. Kinase-deficient Tc PINK1 fails to elicit parkin autoubiquitination/activation and subsequent NLRP3 polyubiquitination. Bars

represent mean ± s.e.m. (n=3). **E,** TUBE assay in iCont and PARKIN-deficient hDA neurons shows polyubiquitination of NLRP3 is abolished upon PARKIN-depletion. Bars represent mean ± s.e.m. (n=3) **F,** TUBE assay in AAV GFP- and AAV GFP-Cre-injected parkin$^{flx/flx}$ ventral midbrain lysates shows polyubiquitination of NLRP3 is abolished upon *in vivo* DA neuron parkin depletion. Bars represent mean ± s.e.m. (n=4). **G,** Overexpression of WT myc-tagged parkin hastens FLAG-NLRP3 clearance, whereas overexpression of the C431S myc-tagged parkin prevents FLAG-NLRP3 clearance, evidenced by a cycloheximide chase assay. Bars represent mean ± s.e.m. (n=3). **H,** Cycloheximide chase assay in iCont and PARKIN-deficient hDA neurons shows that the absence of PARKIN prevents NLRP3 clearance. Bars represent mean ± s.e.m. (n=3).

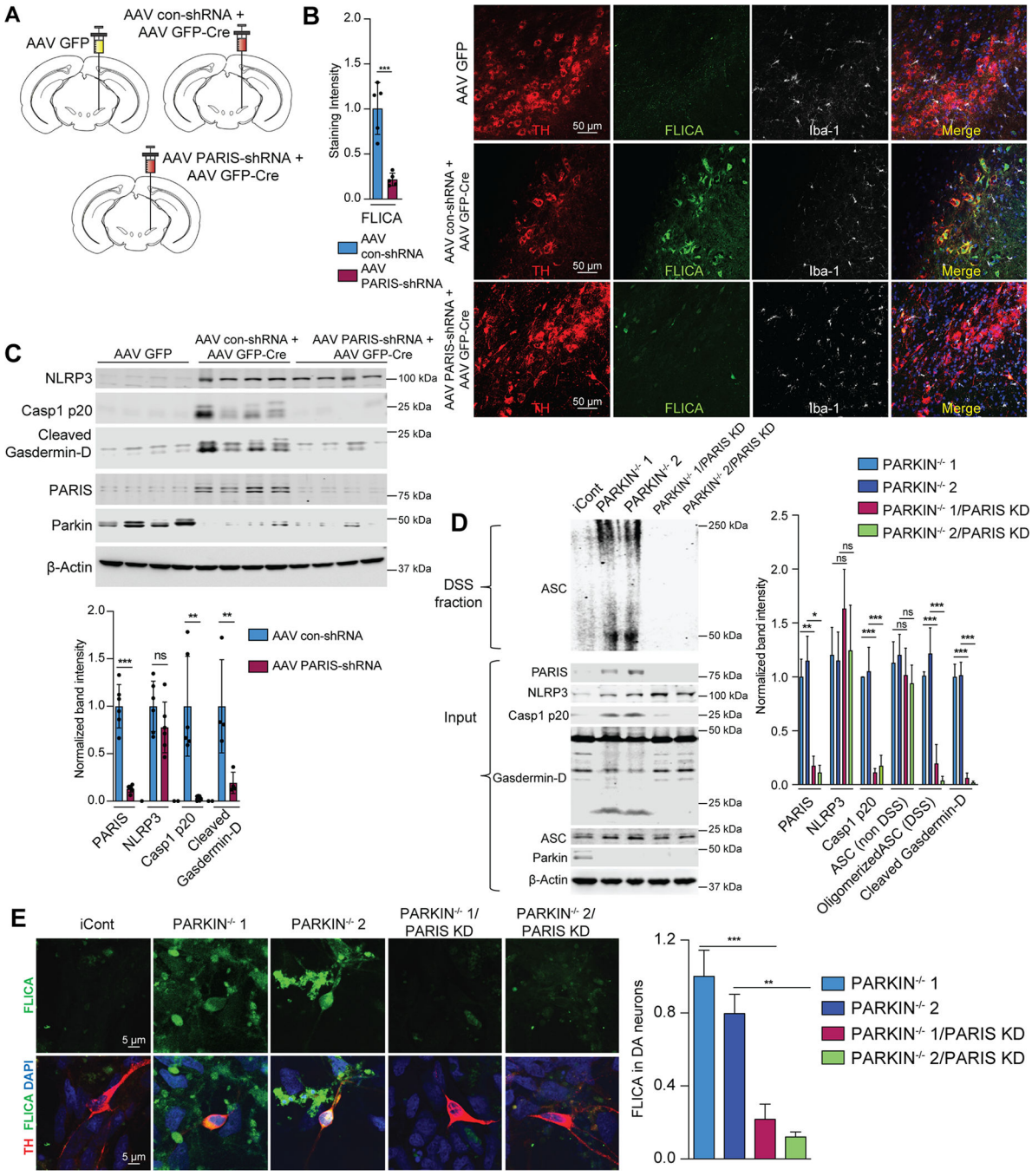

Figure 4: PARIS facilitates inflammasome activation in parkin-depleted DA neurons.

A, Schematic for stereotaxic injection paradigm **B**, *In vivo* FLICA assay demonstrates near complete abrogation of DA neuron Casp1 activity in AAV GFP-Cre-injected parkin$^{flx/flx}$ mice that were co-injected with AAV shRNA-PARIS to prevent PARIS induction. Bars represent mean ± s.e.m. (n=5). **C**, Immunoblot analysis reveals that preventing PARIS induction in the adult-onset DA neuron specific parkin deletion model did not affect inflammasome priming (no significant change in NLRP3 induction), but completely prevented Casp1 activation, evidenced by significantly reduced Casp1 p20 levels as well as

Gasdermin-D cleavage. Bars represent mean ± s.e.m. (n=4 to 6). **D**, CRISPR/Cas9-mediated PARIS knockdown prevents ASC oligomerization in PARKIN deficient hDA neurons, as assayed using DSS-crosslinking assay. Input samples reveal reduced Casp1 and Gasdermin-D cleavage and unchanged NLRP3 induction following PARIS knockdown. Bars represent mean ± s.e.m. (n=3) **E**, PARIS knockdown prevents Casp1 activation in PARKIN deficient hDA neurons, as assayed using the FLICA assay. Live iCont, PARKIN deficient, and PARKIN deficient + PARIS KD DA neurons were stained with the FLICA reagent, then fixed and counterstained with TH. Bars represent mean ± s.e.m. (n=4).

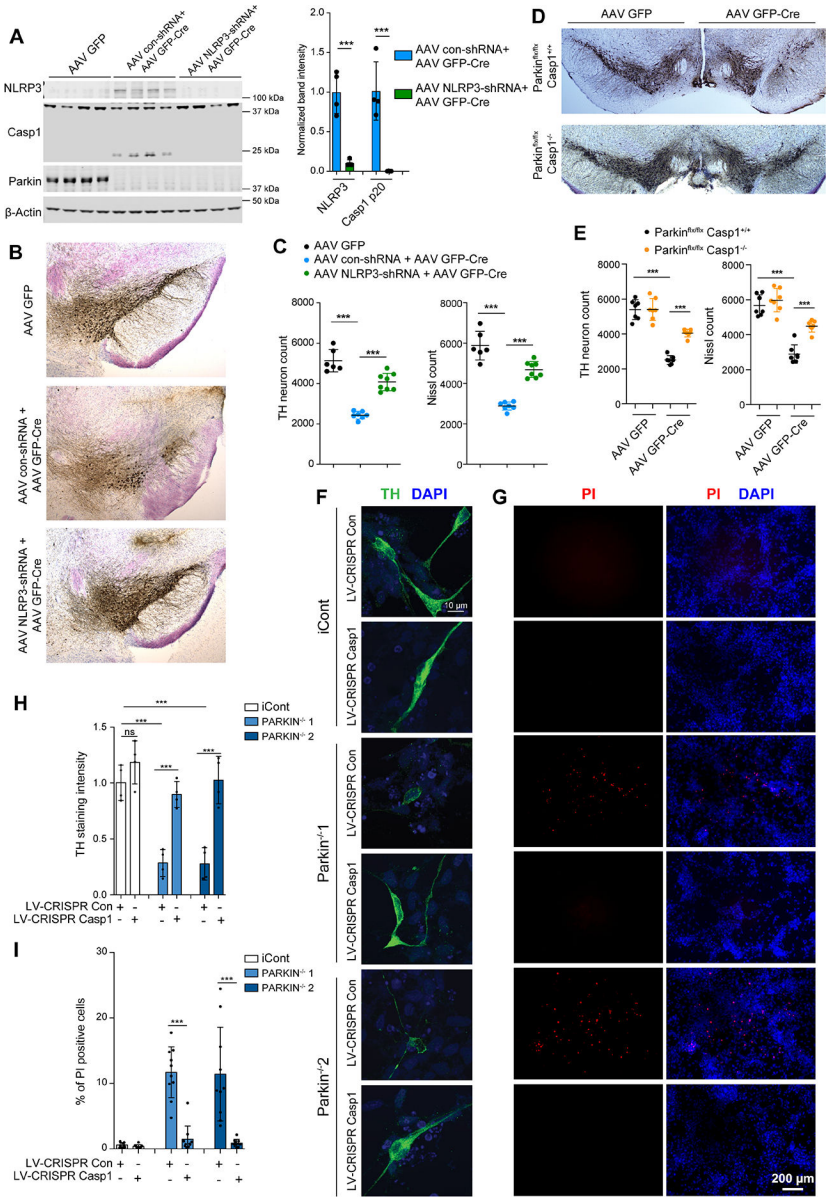

Figure 5: Preventing inflammasome activation protects against loss of parkin-associated neuron death.

A, Immunoblots showing that knocking down of NLRP3 expression via shRNA AAV abrogates Casp1 activation in adult onset, DA neuron parkin depleted mice. Bars represent mean ± s.e.m. (n=4). **B, C,** Representative images, and stereological counting of TH and Nissl positive cells shows significant neuroprotection in AAV NLRP3-shRNA-injected adult onset, DA-neuron parkin depleted mice, when compared to AAV con-shRNA injected control mice. Bars represent mean ± s.e.m. (n=6–8). **D, E,** Representative images and stereological counting of TH and Nissl positive cells shows significant neuroprotection in adult onset, parkin depleted parkin$^{flx/flx}$/ Casp1$^{-/-}$ mice, when compared to littermate control parkin$^{flx/flx}$/ Casp1$^{+/+}$ mice. Bars represent mean ± s.e.m. (n=7). **F, H,** Immunofluorescence for TH in iCont, PARKIN$^{-/-}$ and PARKIN$^{-/-}$+Casp1 KD hDA neurons shows that knockdown of Casp1 prevents the loss of PARKIN-associated reduction

in TH levels. Bars represent mean ± s.e.m. (n=4). **G, I,** PI staining in iCont, PARKIN$^{-/-}$ and PARKIN$^{-/-}$+Casp1 KD hDA neurons shows that knockdown of Casp1 prevents the onset of loss of PARKIN-associated DA neuron death. Bars represent mean ± s.e.m. (n=10).

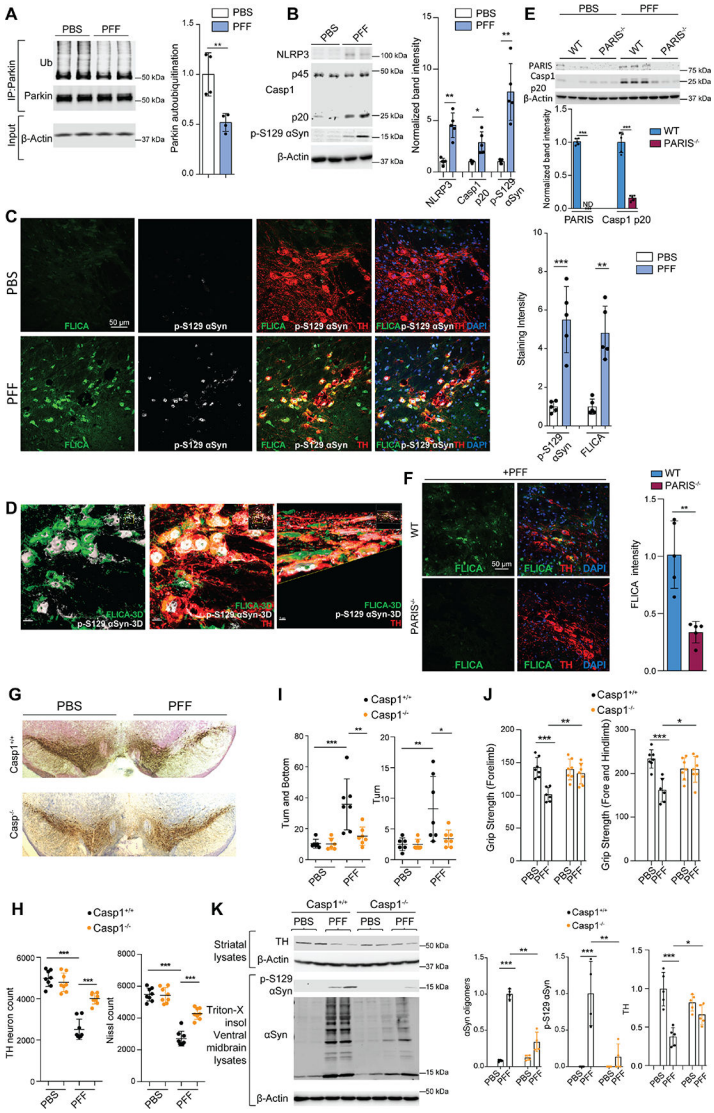

Figure 6: Loss of parkin activity licenses DA neuron NLRP3 inflammasome-dependent neurodegeneration in the α-Syn PFF model.

A, Immunoprecipitation of parkin from PBS and α-Syn PFF-injected mouse ventral midbrain lysates reveals reduced parkin autoubiquitination following α-Syn PFF-subjection, indicating reduction in parkin activity. Bars represent mean ± s.e.m. (n=4). **B,** Immunoblot analysis reveals NLRP3 inflammasome priming and activation in the ventral midbrain lysates of α-Syn PFF-injected mice. Bars represent mean ± s.e.m. (n=5). **C, D,** FLICA staining followed by double immunostaining reveals increased Casp1 activity within TH positive SNpc DA neurons in α-Syn PFF-injected mice. Counterstaining for p-S129-α-Syn shows that many of the neurons harboring α-Syn aggregates are FLICA positive. Bars represent mean ± s.e.m. (n=5). **E,** Immunoblot analysis showing that α-Syn PFF-induced Casp1 activity is significantly reduced in the ventral midbrain lysates of PARIS$^{-/-}$ mice. Bars represent mean ± s.e.m. (n=5). **F,** FLICA staining followed by TH immunostaining reveals abrogation of Casp1 activity in the SNpc DA neurons of α-Syn PFF-injected PARIS$^{-/-}$ mice. Bars represent mean ± s.e.m. (n=5). **G, H,** Stereological counting of TH and

Nissl positive cells shows significant neuroprotection in α-Syn PFF-injected Casp1$^{-/-}$ mice, when compared to Casp1$^{+/+}$ littermate control mice. Bars represent mean ± s.e.m. (n=8). **I, J,** α-Syn PFF-injected Casp1$^{-/-}$ mice exhibit significantly diminished motor deficits, as assayed by performance on the pole test and the grip-strength test. Bars represent mean ± s.e.m. (n=6–7). **K,** Casp1$^{-/-}$ mice are protected from α-Syn PFF-induced TH reduction in the striatum, as well as pathologic p-S129-α-Syn and oligomeric α-Syn accumulation in Triton-X insoluble ventral midbrain lysates, as evidenced by immunoblots. Bars represent mean ± s.e.m. (n=4–5).

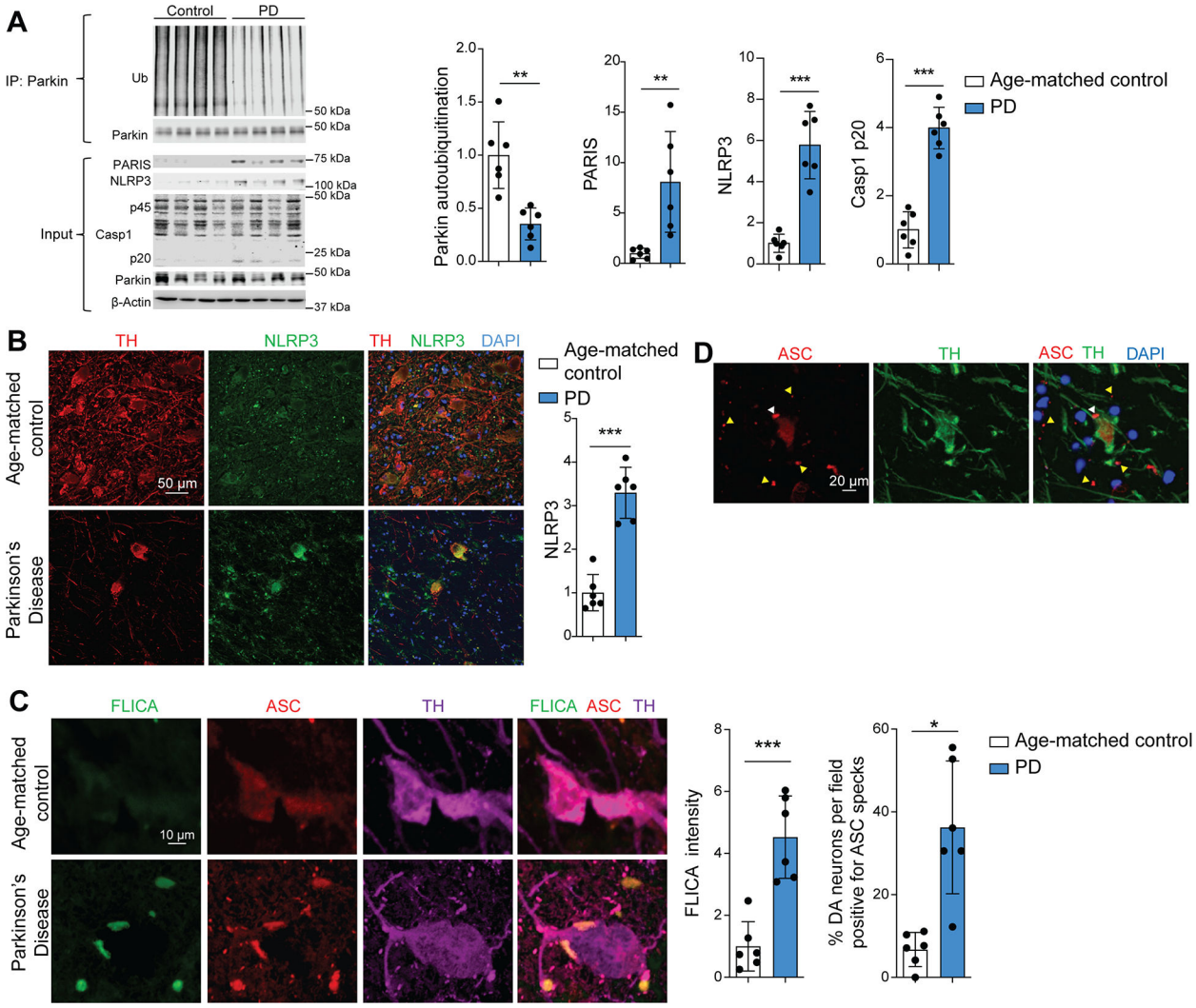

Figure 7: NLRP3 inflammasome activation in Human PD postmortem DA neurons.

A, Immunoblot analysis reveals Parkin inactivation, NLRP3 inflammasome priming and activation in the SNpc lysates of postmortem PD brains. Bars represent mean ± s.e.m. (n=6). **B,** IHC analysis reveals NLRP3 induction within surviving DA neurons in SNpc brain sections from PD patients, compared to age-matched controls. Bars represent mean ± s.e.m. (n=6). **C,** *In vivo* FLICA assay followed by double IHC for TH and ASC showing increased Casp1 activation and ASC speck formation within TH-positive SNpc DA neurons in PD patient SNpc brain sections. Bars represent mean ± s.e.m. (n=6). **D**, Double IHC for TH and ASC shows that SNpc DA neurons (indicated with white arrowhead) as well as other, non-DA cells (indicated with yellow arrowheads) contain ASC specks.

KEY RESOURCES TABLE

REAGENT or RESOURCE	SOURCE	IDENTIFIER
Antibodies		
mouse anti-Caspase-1	Adipogen	Cat# AG-20B-0042-C100 RRID:AB_2755041
mouse anti-NLRP3	Adipogen	Cat# AG-20B-0014-C100 RRID:AB_2885199
mouse anti-parkin or Prk8	Cell Signaling	Cat# #4211 RRID:AB_2159920
rabbit anti-parkin	Cell Signaling	Cat# #2132 RRID:AB_10693040
HRP-conjugated mouse anti-β-actin	Sigma-Aldrich	Cat# A3854 RRID:AB_262011
rabbit anti-TH	Novus	Cat# NB300–109 RRID:AB_10077691
mouse anti-TH	Novus	Cat# MAB7566 RRID:AB_2885201
goat anti-Iba-1	Abcam	Cat# ab5076 RRID:AB_2224402
rabbit anti-Iba-1 (for ICC/IHC)	Wako	Cat# 019–19741 RRID:AB_839504
rabbit anti-Iba-1 (for western blotting)	Wako	Cat# 016–20001 RRID: AB_839506
rabbit anti-ASC	Adipogen	Cat# AG-25B-0006-C100 RRID:AB_2885200
rabbit anti-GFP	Cell Signaling	Cat# #2956 RRID:AB_1196615
rabbit anti- β-actin-HRP	Cell Signaling	Cat# # #5125 RRID: AB_1903890
mouse anti-HA	Thermo Fisher	Cat# # 26183–1MG RRID:AB_2533049
rabbit anti-GST	Cell Signaling	Cat# #2622 RRID:AB_331670
mouse anti-FLAG	Sigma Aldrich	Cat# F3165 RRID:AB_259529
rabbit anti-FLAG	Sigma-Aldrich	Cat# F7425 RRID:AB_439687
mouse anti-myc	Thermo Fisher	Cat# # MA1–980 RRID:AB_558470
rabbit anti-myc	Cell Signaling	Cat# #5605 RRID:AB_1903938
HRP-conjugated mouse anti-myc	Cell Signaling	Cat# #2040, RRID:AB_2148465
rabbit anti-PARIS/ZNF746	Proteintech	Cat# 24543–1-AP RRID:AB_2879598
rabbit anti-Ub	Novus	Cat# NB300–129 RRID:AB_2180545
rabbit anti-pS129 α-Synuclein	Abcam	Cat# ab51253 RRID:AB_869973
mouse anti-pS129 α-Synuclein	Wako	Cat# 015–25191 RRID:AB_2537218

REAGENT or RESOURCE	SOURCE	IDENTIFIER
rabbit anti-PINK1	Cell Signaling	Cat# #6946 RRID:AB_11179069
rabbit anti-alpha tubulin	Cell Signaling	Cat# #2144 RRID:AB_2210548
mouse anti-IL-1β	Cell Signaling	Cat# #12242 RRID:AB_2715503
rabbit anti-IL-18	Cell Signaling	Cat# #54943 RRID:AB_2909592
mouse Gasdermin-D	Adipogen	Cat# AG-25B-0036-C100 RRID:AB_2909593
rabbit Htra2	Cell Signaling	Cat# # 2176, RRID:AB_2122848
mouse anti-TUJ1	R&D Systems	Cat# MAB1195 RRID:AB_357520
IRDye 800 Goat anti-Mouse IgG Secondary Antibody	LiCor	Cat# 926–32210 RRID:AB_621842
IRDye 800 Goat anti-Rabbit IgG Secondary Antibody	LiCor	Cat# 926–32211 RRID:AB_621843
IRDye 680 Goat anti-Mouse IgG Secondary Antibody	LiCor	Cat# 926–68070 RRID:AB_10956588
IRDye 680 Goat anti-Rabbit IgG Secondary Antibody	LiCor	Cat# 926–68071 RRID:AB_10956166
Bacterial and Virus Strains		
lentiCRISPR v2		Addgene Cat# 52961
One Shot™ Stbl3™ Chemically Competent E. coli	Thermo Fisher	Cat# C7373–03
Biological Samples		
Post-mortem SNpc tissue from PD patients and age-matched control subjects	This paper (Table S1)	N/A
Chemicals, Peptides, and Recombinant Proteins		
1X PBS pH 7.4	Quality Biologicals	Cat# 114–058-101
10X TBS pH 7.4	Quality Biologicals	Cat# 351–086-101
Protease Phosphatase Inhibitor Cocktail	Cell Signaling	Cat# #5872
Paraformaldehyde (PFA) reagent grade	Sigma	Cat# P6148
D.P.X.	Sigma	Cat# 317616
Thionin acetate salt	Sigma	Cat# T7029
Normal donkey serum	Jackson ImmunoResearch	Cat# 017–000-121
MCC-950 Sodium Salt	Adipogen	Cat# AG-CR1–3615-M050
PLX5622 (batch#98636)	Med Chem Express	Cat# HY-114153
VECTASHIELD HardSet Antifade Mounting Medium	Vector laboratories	Cat# H-1400–10
SIGMAFAST(TM) 3,30-Diaminobenzidine tablets	Sigma	Cat# D4293
Recombinant UBE1	Boston Biochem,	Cat# E-305
Recombinant UbcH7	Boston Biochem	Cat# A-640
Recombinant Parkin	Generated in-house (Lee et al., 2017)	N/A
Recombinant Tc PINK1	Boston Biochem	Cat# AP-180

REAGENT or RESOURCE	SOURCE	IDENTIFIER
Recombinant NLRP3	Abcam	Cat# ab198069
Recombinant GST protein	Sigma	SRP5348–20UG
His-Ub	Boston Biochem,	Cat# U-530
DSS (disuccinimidyl suberate)	Thermo Fisher	Cat# 21655
MG-132	Millipore Sigma	Cat# M7449–1ML
Fetal Bovine Serum	HyClone™	Cat # SH30070.03HI
Penicillin-Streptomycin solution	Sigma	Cat # P4333
TrypLE Express	Gibco	Cat # 12604–013
DMEM Media	Gibco	Cat # 11965–092
Critical Commercial Assays		
PolyFect Transfection Reagent	Qiagen	Cat# 301105
FAM-FLICA Caspase-1 (YVAD) Assay Kit	Immunochemistry Technologies	Cat# 97
Anti-FLAG M2 Magnetic Beads	Sigma	Cat# M8823
Myc-Trap Agarose	Chromotek	Cat# yta-10
Vectastain Elite ABC Kit (Peroxidase, Rabbit IgG)	Vector laboratories	Cat# PK-6101
Vectastain Elite ABC Kit (Peroxidase, Mouse IgG)	Vector laboratories	Cat# PK-6102
Pierce LAL chromogenic endotoxin quantitation kit	Thermo Scientific	Cat# 88282
Pierce BCA protein assay kit	Thermo Scientific	Cat# 23227
DreamTaq Green PCR Master Mix (2X)	Thermo Scientific	Cat# K1082
EasySep™ Mouse CD11b Positive Selection Kit II	StemCell Technologies	Cat# #18970A
SYBR™ Green PCR Master Mix	Applied Biosystems	Cat# 4344463
High-Capacity cDNA Reverse Transcription Kit	Applied Biosystems	Cat# 4368814
UbiTest Magnetic TUBE Elution Kit	Life Sensors	Cat# 0411M-1000
Deposited Data		
Experimental Models: Cell Lines		
SH-SY5Y cell line	ATCC	ATCC CRL-2266
Experimental Models: Organisms/Strains		
C57BL/6J	Jackson Laboratory	Stock No: 000664
$Nlrp3^{A350VneoR}$ (NLRP3 knock-in)	Jackson Laboratory	Stock No: 017969
Casp1 deficient ($Casp1^{-/-}$) mice	Jackson Laboratory	Stock No: 016621
Nlrp3 deficient ($NLRP3^{-/-}$) mice	Jackson Laboratory	Stock No: 021302
$Parkin^{flx/flx}$ / Exon 7 floxed parkin mice	Generated in-house (Shin et al., 2011)	N/A
PARIS deficient (PARIS/$ZNF746^{-/-}$) mice	Generated in-house (Brahmachari et al., 2019)	N/A
Oligonucleotides		
$Nlrp3^{A350VneoR}$ (NLRP3 knock-in) mutant forward 5'-GCT ACT TCC ATT TGT CAC GTC C-3'	Jackson Laboratory	12834
$Nlrp3^{A350VneoR}$ (NLRP3 knock-in) wild-type forward 5'CAC CCT GCA TTT TGT TGT TG-3'	Jackson Laboratory	14584

REAGENT or RESOURCE	SOURCE	IDENTIFIER
Nlrp3^{A350VneoR} (NLRP3 knock-in) common 5'CGT GTA GCG ACT GTT GAG GT-3'	Jackson Laboratory	14585
Casp1 wild-type forward 5'GAG ACA TAT AAG GGA GAA GGG-3'	Jackson Laboratory	12572
Casp1 mutant forward 5'TGC TAA AGC GCA TGC TCC AGA CTG-3'	Jackson Laboratory	oIMR5944
Casp1 common 5'ATG GCA CAC CAC AGA TAT CGG-3'	Jackson Laboratory	12573
Nlrp3 mutant forward 5'TGC CTG CTC TTT ACT GAA GG-3'	Jackson Laboratory	16568
Nlrp3 WT forward 5'TCA GTT TCC TTG GCT ACC AGA-3'	Jackson Laboratory	16703
Nlrp3 common 5'TTC CAT TAC AGT CAC TCC AGA TGT-3'	Jackson Laboratory	16704
CRISPR-Cas9 Casp1 knockdown constructs	This paper, (Table S2)	N/A
q-RT PCR primers for NLRP3, Casp1, β-actin	This paper, (Table S3)	N/A
Recombinant DNA		
AAV-GFPCre (AAV serotype 2) AAV	Vector Biolabs	Cat# 7016
AAV-GFP (AAV serotype 2) AAV	Vector Biolabs	Cat# 7004
AAV2-GFP-U6-m-NLRP3-shRNA	Vector Biolabs	N/A
AAV2-GFP-U6-m-con-shRNA	Vector Biolabs	N/A
pcDNA3-N-Flag-NLRP3	(Shi et al., 2016)	Addgene Cat# 75127
pcDNA3-N-Flag-NLRP3 1–90	(Shi *et al.*, 2016)	Addgene Cat# 75137
pcDNA3-N-Flag-NLRP3 91–710	(Shi *et al.*, 2016)	Addgene Cat# 75140
pcDNA3-N-Flag-NLRP3 711–1034	(Shi *et al.*, 2016)	Addgene Cat# 75141
Software and Algorithms		
ImageJ 1.51	National Institute of Health (NIH)	https://imagej.nih.gov/ij/
GraphPad Prism 6	GraphPad Software	https://www.graphpad.com/scientific-software/prism/
Microsoft Excel 2016	Microsoft Corporation	https://products.office.com/en-US/
IMARIS	Bitplane	https://imaris.oxinst.com/
ZEN lite	Zeiss	https://www.zeiss.com/microscopy/us/products/microscope-software/zen.html
Stereo Investigator software	MBF Bioscience	https://www.mbfbioscience.com
Other		
2X Laemmli Sample Buffer	Bio-Rad	Cat# 1610737
Novex WedgeWell 8–16% Tris-Glycine Mini Gels	Thermo Scientific	Cat# XP08165BOX
Novex WedgeWell 4–20% Tris-Glycine Mini Gels	Thermo Scientific	Cat# XP04205BOX
SUPERSIGNAL WEST PICO PLUS	Thermo Scientific	Cat# 34580
Nitrocellulose Membrane	Bio-Rad	Cat# 1620115